

Reply to Referee reviews

Manuscript title

Comparison of different methods to retrieve effective snow grain size in central Antarctica

Date of reply

31 July 2017

5

Dear Reviewers,

thank you for the helpful comments and suggestions on improving the manuscript.

The detailed replies to your comments (highlighted in gray) are given below, followed by the specific changes made in the manuscript (changes are highlighted in bold text). The marked-up version (see below) illustrates all changes made compared

10 to the manuscript published in The Cryosphere Discussions.

Kind regards from the authors.

Replies to comments of Referee 1 (E. Zege)

Page 8, Lines 3-6:

The large uncertainty of the SGSP retrieval for high solar zenith angles is related to the conversion of the measured reflectance from one viewing direction by the satellite sensor into measured albedo. For this, the bidirectional reflectance distribution function (BRDF) of the snow surface has to be assumed.

This statement is incorrect. 'The conversion of the measured reflectance from one viewing direction by the satellite sensor into measured albedo' is not used in the SGSP algorithm. Actually in the SGSP algorithm, the angular dependency in the registered signals is excluded using registration of the signal for additional wavelength, and no assumptions about BRDF is used. It is one of the main advantages of this technique.

15 Thank you for pointing out this formulation mishap. What we intended to say here is related to the surface albedo model and not the conversion of the measured radiance into albedo. The assumption on the particle form factor and approximation of the photon escape function which defines the angular behavior of the light reflected from a medium can be less accurate for oblique illumination angles. Similarly, as can be seen from Zege et al. (2011) Fig. 1, the slight dependence of the phase function on the wavelength is angle dependent. This means that for some angles the assumption of the spectrally constant BRDF shape holds

better than for others, which may explain the diurnal cycle of the retrieved snow grain size discussed below. These details have been included in the manuscript.

Changes in manuscript:

- 5 After a preliminary separation of snow pixels, the effective snow grain size of each pixel is retrieved from radiance measurements of MODIS channels 3 (469 nm wavelength), 2 (858 nm), and 5 (1240 nm). **Assuming a spectrally constant bidirectional reflectance distribution function (BRDF) of snow and using the combination of three spectral channels, the angular dependency of the measured radiance is excluded.**
- (...)
- 10 **The large uncertainty of the SGSP retrieval for high solar zenith angles is related to the assumptions on the particle form factor A and the approximation of the escape function $K_0(\theta_0)$ which is less accurate for oblique illumination angles. In combination with the strong forward scattering characteristic for snow grains, small errors in the assumed A and $K_0(\theta_0)$ can greatly distort the albedo. Similarly, the spectral behavior of the BRDF of snow slightly depends on the illumination angle (Zege et al., 2011).** Consequently, within this work the satellite retrieval is limited to $\theta_0 \leq 75^\circ$.

P.8, Lines 6- 7:

Due to the strong forward scattering characteristic for snow grains, small errors in the assumed BRDF greatly distort the albedo, especially at low sun elevations

Correspondingly, this sentence should be corrected, because there is no use of 'assumed BRDF' in SGSP procedure.

- 15 Similar to above, this sentence referred to the assumptions on particle form factor and the assumption that the BRDF shape does not change with the wavelength. This has been reformulated (see above).

P.10, Fig 5:

Fig. 5 presents important data. For more fast understanding and analysis it would be very useful to give the corresponding Sun polar angles as the second scale at X- axis.

Thank you for this suggestion. We adjusted Fig. 5 accordingly.

Changes in manuscript:

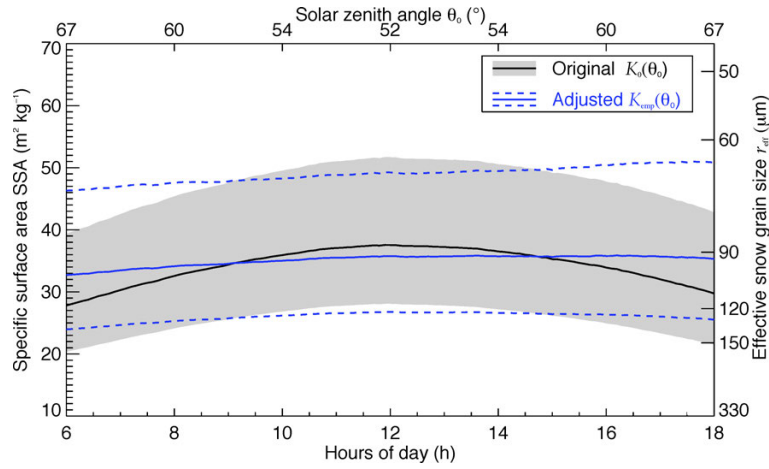


Figure 5 shows the results retrieved from ground-based measurements with CORAS (SSA and effective snow grain size) on 24 December 2013 between 6 UTC and 18 UTC. **During this time, the solar zenith angle varied between 52° and 67°.**

P.10, Lines 7-8:

As no snowfall occurred on that day, the diurnal cycle is likely to be an artifact originating from the change in solar zenith angle and the assumed escape function $K_0(\theta_0)$.

It might be a very interesting and useful observation. In all cases it makes a reader think about necessity to use more accurate approximation of the $K_0(\theta_0)$ function for interpretation data at low Sun positions. The recommended formula

$$K_{\text{emp}}(\theta_0) = \frac{3}{7}(1.5 + 1.1 \cos \theta_0) = \frac{2}{7}(1 + 0.73 \cos \theta_0)$$

should be rather taken as empirical approximation for considered case. This result requires a more detail consideration in future studies.

Yes, we agree and have corrected the manuscript accordingly. The equation given in the manuscript was derived purely from empirical analysis of the diurnal time series of this single case and is likely not valid in other cases. For a more general adjustment of the escape function, a more careful consideration must indeed be performed. However, this is out of the scope of this work, but should be addressed in future studies using explicit BRDF measurements.

Changes in manuscript:

The analysis of measurements during other cloudless days showed similar features. Therefore, K_{emp} was applied for the entire period of measurements. **However, it should be noted that the escape function K_{emp} from Eq. 13 is an empirical approximation for the cases investigated here. To derive a more general description of the escape function, more cases and explicit BRDF measurements are needed, which is beyond the scope of this study.**

P.10, Lines 8-10:

The escape function might be incorrect if the snow BRDF is more complex due to the non-spherical snow grain shape.

This statement is incorrect. More accurate would be 'The used approximation (3) for escape function might be incorrect for snow at very oblique incidence because of its very elongated phase function'.

Thank you for this comment. Indeed, the oblique angles are problematic because of the strong forward scattering phase function and any inaccuracies in the approximation will have a greater effect at these angles. At the same time, we meant to highlight the importance of the correct selection of the form factor, that is, the asymmetry parameter and the absorption enhancement parameter at this point. We have changed the text to accommodate for these details.

5 **Changes in manuscript:**

The approximation for the escape function (Eq. 4) might be incorrect for snow at oblique incidence due to its elongated phase function. At the same time, a representative form factor A is required to account for the non-spherical snow grain shape.

P.11, Lines 24-25:

Therefore, each instrument retrieves the effective grain size from a different depth within the snowpack.

Moreover, even the same instrument takes measurements from layers with different depth dependent on wavelength. All retrievals considered in this paper (and in many others) were performed neglecting snow layer stratification.

This statement is true. We included this comment to foster reading comprehension.

10 **Changes in manuscript:**

All retrievals considered in this study were performed neglecting snow layer stratification.

P.13, Line 4:

*which can be related to snowfall of about **1mm** at Kohnen*

Do authors really mean '1mm'?

Yes, we indeed mean snowfall of about 1 mm. This is an approximate value which stems from visual estimation as no quantitative measurements were performed during the observations. In the dry atmosphere over the high Antarctic plateau, precipitation events with less than a few mm depth are common.

15 **Changes in manuscript:**

(...) which can be related to snowfall of about 1 mm at Kohnen (**visual estimation**).

Abstract P.1:

The effective size of snow grains affects the reflectivity of snow surfaces and thus the local surface energy budget in particular in polar regions. Therefore, the specific surface area (SSA) was monitored.

There is some breach of logic: 'The effective size of snow grains affects... Therefore, the specific surface area (SSA) was monitored.' Still it is not stated how these quantities are related.

Thank you for pointing this out, we changed this part of the abstract to avoid this breach of logic.

Changes in manuscript:

The size of snow grains affects the reflectivity of snow surfaces and, thus, the local surface energy budget in particular in polar regions. Therefore, the specific surface area (SSA) **as an equivalent measure for snow grain size** was monitored for a two-month period in central Antarctica (Kohnen research station) during austral summer 2013/14.

P.2, Line 5:

For example, Munneke et al. (2008) found variations of the broadband albedo of snow at five different locations in Dronning Maud Land in a range between 0.77 and 0.88.

I recommend small change:

'For example, Munneke et al. (2008) found variations of the broadband albedo of snow in a range between 0.77 and 0.88 at five different locations in Dronning Maud Land.'

Thank you. We changed it as suggested.

P.2, Line 3-7:

*However, the snow surface albedo varies both on a temporal and spatial scale. For example, Munneke et al. (2008) found variations of **the broadband albedo** of snow at five different locations in Dronning Maud Land in a range between 0.77 and 0.88.*

*This variability is caused by different parameters such as snow grain size (and shape), surface roughness (e.g., Warren et al., 1998), soot content (e.g., Bond et al., 2013), and cloudiness; **it depends on wavelength**... and solar position.*

Because the first sentence is only about the broadband albedo, the second sentence is required to be corrected.

This is correct, thank you for pointing it out. We adjusted the manuscript accordingly.

Changes in manuscript:

Changes of broadband and spectral snow albedo are caused by different parameters such as snow grain size (and shape), surface roughness (e.g., Warren et al., 1998), soot content (e.g., Bond et al., 2013), and cloudiness. **It further depends on wavelength** (e.g., Hudson et al., 2006; Warren and Brandt, 2008) **as well as** solar position (e.g., Wiscombe and Warren, 1980;

Wiscombe, 1980; Dumont et al., 2010) **and varies with snow depth (e.g., Wiscombe and Warren, 1980) and liquid water content (e.g., Wiscombe and Warren, 1980; Gallet et al., 2014).**

Replies to comments of Referee 2 (G. Picard)

Overall the paper is quite short. The authors should address in their response to reviewers the reason why this study is not merged with the paper in preparation (Freitag et al.). The review of the literature is also relatively light and should be completed (see some personal suggestions below, but works from other groups should be considered as well). The discussion should be completed with an analysis of the results with respect to other previous studies.

The reason why these two studies are not merged are the different focuses of both studies. While the manuscript discussed here compares methods to retrieve effective snow grain size from different remote sensing platforms, the manuscript in preparation by Freitag et al. focuses on the seasonal evolution of SSA at Kohnen station and concentrates on the microphysical processes within the snowpack. Merging both studies would produce synergy effects but rather weaken the visibility of each individual study. In our manuscript, the in situ dataset is only used for validation of the remote sensing results. Of course, time series and changes of SSA are discussed but any analysis of the microphysical processes causing these changes are beyond the scope of our study. In the opinion of the authors, this justifies separate manuscripts.

The comments on the literature review and the discussion are considered within the specific comments.

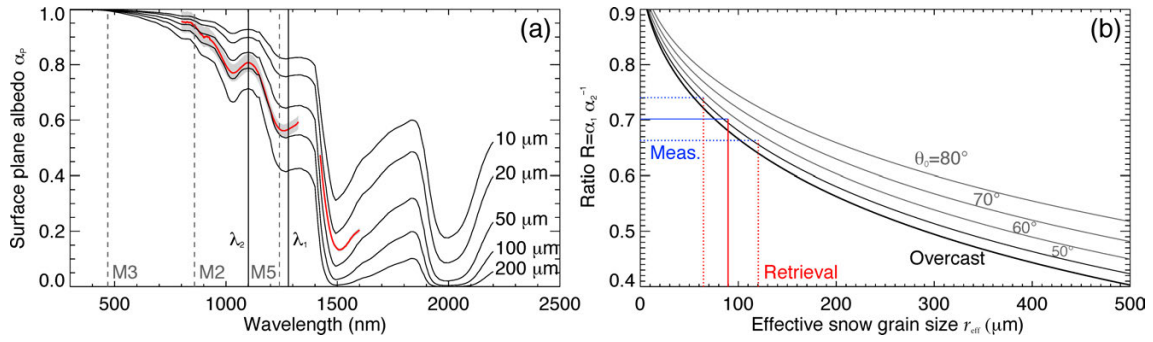
Uncertainties are given at different stages of the methodology, which is very useful, but the way these uncertainties have been estimated is not described, and they seems to me often overoptimistic. Even though it is notoriously difficult to estimate uncertainties, some justification are required. In addition, the authors do not consider the effect of the roughness, and they neglect the impact of wavelength-dependent errors of spectra calibration on the ratio R . Both are probably not negligible and should be evaluated or at least indicated.

We have revised the uncertainty estimation and its description to make clear where the uncertainties of each measurement result from. The changes made in the manuscript are stated at the corresponding specific comments.

The paper does not show albedo spectra from which SSA are derived. Given the focus of the paper, it could be acceptable. Nevertheless I suggest to add example of spectra for one date to illustrate the derivation of SSA from albedo and to possibly help in the analysis of the bias observed between the airborne timeseries and other time-series which remains unexplained.

We agree that showing a measured spectral albedo can further illustrate the derivation of SSA. We therefore included a spectral albedo measured by CORAS on 24 December 2013 (14 UTC) in Fig. 4a and adapted the simulated snow surface plane albedos to the solar zenith angle of the time of measurement (around 54°). In addition, we modified Fig. 4b as follows: for the illustration of retrieved r_{eff} from the ratio \mathcal{R} we now use the ratio computed from the spectral albedo by CORAS as shown in Fig. 4a.

Changes in manuscript:



Left (a): Surface plane albedo for effective snow grain sizes between 10 μm and 200 μm , $\theta_0 = 54^\circ$, $A = 5.8$, χ -data from Warren and Brandt (2008). M3, M2, and M5 mark MODIS spectral bands used within the SGSP algorithm. λ_1 and λ_2 denote wavelengths used within the CORAS and SMART grain size retrieval. **The read solid line and shaded gray show a spectral albedo measured by CORAS on 24 December 2013 (14 UTC).** Right (b): Illustration of retrieval principle. dependence of ratio \mathcal{R} with respect to effective snow grain size for different solar zenith angles (50° to 80°) and for overcast conditions, $A = 5.8$, χ -data from Warren and Brandt (2008). Blue and red lines illustrate the retrieval of effective snow grain size from a measured albedo ratio $\mathcal{R} = 0.7$ with a relative uncertainty of 5.5 %.

Furthermore, a spectral albedo between 700 nm to 1600 nm wavelength measured by CORAS on 24 December 2013 (14 UTC) is shown. The data gap between 1300 nm and 1400 nm wavelength is resulting from low signal-to-noise ratios at these wavelengths.

Applying Eq. 12 to the spectral albedo measured by CORAS on 24 December 2013 (Fig. 4a), the measured ratio \mathcal{R} of 0.702 ± 0.039 leads to an estimated effective snow grain size of about $90 \pm 31 \mu\text{m}$ at $\theta_0 = 54^\circ$ (blue and red lines in Fig. 4b).

To foster comparison in the future, I recommend to publish the four timeseries once the paper is accepted.

- 15 This is a valuable comment, thank you. Indeed, we have already planned to publish the following three time series of SSA in the Publishing Network for Geoscientific & Environmental Data (PANGAEA) : CORAS, SMART, MODIS.

This will be done as soon as the manuscript is published.

Abstract:

The term 'effective size of snow grain' is not well defined, especially 'effective' is relative to the domain (optics, microwave, chemistry, etc). Optical grain size is more adequate.

This is correct. The definition of the term 'effective size of snow grains' was described too late. We therefore refrain from using 'effective' within the abstract already. Instead, we introduce the study in the abstract on the basis of the SSA alone.

Additionally, we carefully revised the use of 'effective' . If the quantity of 'effective snow grain size' is used, 'effective' is included. If, in general, we refer to the size of snow grains without explicitly pointing to a physical quantity, 'effective' is omitted.

Changes in manuscript:

- 5 **The size of snow grains** affects the reflectivity of snow surfaces and, thus, the local surface energy budget in particular in polar regions. Therefore, the specific surface area (SSA) **as an equivalent measure for snow grain size** was monitored for a two-month period in central Antarctica (Kohnen research station) during austral summer 2013/14.

(...)

~~(vice-versa for r_{eff}),~~

- 10 (...)

~~(overestimation of r_{eff})~~

Abstract:

The abstract tells what has been done, but is not an abstract of the paper. The objective of the study is missing, as well as the conclusion.

We revised the abstract accordingly.

Changes in manuscript:

- 15 The size of snow grains affects the reflectivity of snow surfaces and, thus, the local surface energy budget in particular in polar regions. Therefore, the specific surface area (SSA) **as an equivalent measure** for snow grain size was observed for a two-month period in central Antarctica (Kohnen research station) during austral summer 2013/14. The data were retrieved on the basis of ground-based spectral surface albedo measurements collected by the COmpact RAdiation measurement System (CORAS) and airborne observations with the Spectral Modular Airborne Radiation measurement sysTem (SMART). **The Snow Grain Size and Pollution amount (SGSP) algorithm, originally developed to analyze spaceborne reflectance measurements by**
- 20 **the MODerate Resolution Imaging Spectroradiometer (MODIS), was modified in order to reduce the impact of the solar zenith angle on the retrieval results and to cover measurements in overcast conditions.** Spectral ratios of surface albedo at 1280 nm and 1100 nm wavelength were used to reduce the retrieval uncertainty. The retrieval was applied to the ground-based and airborne observations and validated against optical in situ observations of SSA utilizing an IceCube device. The SSA retrieved from CORAS observations varied between $27 \text{ m}^2 \text{ kg}^{-1}$ and $89 \text{ m}^2 \text{ kg}^{-1}$. Snowfall events caused distinct
- 25 relative maxima of the SSA which were followed by a gradual decrease in SSA due to snow metamorphism and wind-induced transport of fresh fallen ice crystals. **The ability of the modified algorithm to include measurements in overcast conditions improved the data coverage especially at times when precipitation events occurred and the SSA changed quickly.** SSA retrieved from measurements with CORAS and MODIS agree with the in situ observations within the ranges given by the measurement uncertainties. However, SSA retrieved from the airborne SMART data underestimated the ground-based results
- 30 by a factor of 2.

P2 L3:

'most of the sea ice are covered with snow with little seasonal variability'. The variability of sea ice is huge in Antarctica.

Thanks for pointing out this potential misconception. We did not mean the variability of sea ice, but of the snow cover on the sea ice. We reformulated the sentence.

Changes in manuscript:

In Antarctica, more than 99.8 % of the continent and most of the sea ice are covered with snow **all year round** (Burton-Johnson
5 et al., 2016).

P2 L9:

'Furthermore, snow surface albedo varies with snow depth and the liquid water content'. Need a reference for each effect. The dependence to snow depth is almost irrelevant in Antarctica.

Thank you. We added exemplary references for the two parameters influencing the snow surface albedo. The importance of the dependence on snow depth for the study is indeed small, however, we mention this parameter for comprehension.

Changes in manuscript:

It further depends on wavelength (e.g., Hudson et al., 2006; Warren and Brandt, 2008) **as well as** solar position (e.g., Wis-
10 combe and Warren, 1980; Wiscombe, 1980; Dumont et al., 2010) and varies with snow depth (e.g., **Wiscombe and Warren, 1980**) and liquid water content (e.g., **Wiscombe and Warren, 1980; Gallet et al., 2014**).

P2 L11:

Add references of published works (Libois et al., Munneke et al., Picard et al., Pirrazini et al., Warren and co, Zender and co, etc).

We added some additional references to demonstrate the influence of snow grain size on snow albedo.

Changes in manuscript:

From these parameters, the snow grain size has the largest effect on snow albedo. **Simulations by Wiscombe and Warren**
15 **(1980) showed that the spectral albedo in the near-infrared part of the spectrum may drop by a factor of 2 or more when the snow grain size increases from 50 μm to 1000 μm .** Dang et al. (2015) showed that the transition from fresh fallen snow with a typical effective grain size of 100 μm to **aged** snow (1000 μm) leads to a decrease in snow albedo (spectrally integrated over 0.3-4.0 μm) of 15 % from 0.83 to 0.72. **This relation could clearly be identified in ground-based measurements by Domine et al. (2006) analyzing snow samples taken at Svalbard in 2001. They measured a decrease in reflectance at**
20 **1310 nm wavelength by 45 % with increasing grain size from 290 μm to 1175 μm . Libois et al. (2015) and Picard et al. (2016) retrieved a three-year time series of SSA from spectral albedo measurements at Dome C, Antarctica, which**

emphasized the dynamical evolution of near-surface SSA by displaying a 3-fold decrease every summer in response to the increase of air temperature. A detailed comparison of this dataset with snow model simulations and a geophysical interpretation are presented by Libois et al. (2015). Similar seasonal variations but little year-to-year variation was found by Jin et al. (2008) who retrieved snow grain size from measurements with the MODerate Resolution Imaging Spectroradiometer (MODIS) at 1.64 and 0.64 μm over the Antarctic continent for four days each year between 2000 and 2005. Therefore, a positive feedback mechanism can be postulated: increasing snow temperatures are followed by an accelerated snow metamorphism and a decrease of the snow albedo, which leads to higher absorption and heating of the snow. However, the expected snow albedo decrease due to temperature-induced metamorphism (0.3 % for a warming of 3 K) can be overcompensated by an increase in snow albedo by 0.4 % owing to a projected increase in precipitation during the twenty-first century in interior Antarctica (Picard et al., 2012).

P2 L18:

Are these values here for optical grain size ? Is the reference about optical grain size or other grain size metrics ? The sentence should be more precise about this.

The reference is about the geometric grain size (visually determined by means of a magnifying glass). We added this information in the manuscript.

Changes in manuscript:

Observations showed that the **geometric** grain size (**from visual determination**) of snow crystals varies between 10 μm for fresh fallen snow and up to 3 mm for **aged** snow (Singh, 2001).

P3 L7:

It is not clear if the sentence is about the impact of the albedo-grain shape or BRDF-grain shape. Both are quite different and have different impact depending on the algorithm used for the retrieval. For the former issue, the value of 2.6 is extreme. See Kokhanovsky and Zege 2004, Picard et al. 2009, Libois et al. 2013 for other works on this question.

The study of Dang et al. (2016) deals with the influence of grain shape on the snow albedo, not the BRDF. Among other things, Dang et al. (2016) simulate the spectral albedo at 1300 nm wavelength for non-spherical snow grains (with aspect ratio 1) and spherical snow grains. A measured albedo of 0.59 would cause a retrieved effective radius of 60 μm (spherical) or 144 μm (nonspherical). Therefore, the representation of non-spherical snow grains by a population of spherical grains with the same area-to-mass ratio can lead to an underestimation of the effective snow grain size by a factor of 2.4.

Thank you for the suggested references. We want to take this opportunity and included a second reference on this question.

Changes in manuscript:

These albedo models mostly assume spherical grains, which is **unrealistic** because the grain shape is usually far from being spherical (e.g., Kokhanovsky and Zege, 2004; Libois et al., 2013; Leppänen et al., 2015). Picard et al. (2009) estimated an

uncertainty of $\pm 20\%$ when determining SSA from albedo measurements in case of an unknown snow grain shape. A common approach to account for the non-spherical shape of snow grains is to represent the non-spherical snow grains by a population of spherical grains with the same area-to-mass ratio in the spectral albedo model. However, as shown by Dang et al. (2016), this approximation can lead to an underestimation of the retrieved effective snow grain size by a factor of more than 2.

About P3, Libois et al. 2015 and Picard et al. 2016 (both in The Cryosphere), have produced time-series of SSA (3 years) at Dome C in Antarctica which seems relevant to the present study. See also Jin et al. 2008 and Picard et al. 2012 for earlier (and shorter) time-series of SSA in-situ and satellites measurements.

This is true, thank you. We added the suggested studies to the introduction.

Changes in manuscript:

See comment above about P2L11.

P3 L12-13:

'However, polar orbiting satellites do not provide a sufficiently high temporal resolution that may resolve snow precipitation events and snow metamorphism that typically can advance in a matter of hours'. With the number of satellites (MODIS, Sentinel, SSM/I, AMSU, ...) and the convergence of the orbits in the polar regions, subdaily resolution can be achieved.

This is true, in theory a subdaily resolution could be achieved. However, to our knowledge no hourly satellite products of snow grain size are currently available. We rephrased the sentence in order to make it less definitive.

Changes in manuscript:

Up to now, grain size products of polar orbiting satellites do not provide a sufficiently high temporal resolution that may resolve snow precipitation and metamorphism that typically can advance in a matter of hours.

P4L8:

According to Gallet et al. 2009, IceCUBE (i.e. DIFUSSS with 1300 nm only) can not be used from SSA of $60\text{ m}^2/\text{kg}$ and above. If the "in prep" paper shows different results, it would be interesting to add a sentence here. Otherwise the limitation should be indicated.

Thank you for indicating that this limitation was not yet stated in the manuscript. However, the snow samples for which Gallet et al. (2009) reported problems with SSA of $60\text{ m}^2\text{ kg}^{-1}$ and above were all of low density below 100 kg m^{-3} . Within this study, the density of the snow samples used for the SSA measurements were all well above 100 kg m^{-3} (around 60 % of the samples with densities between $280\text{--}350\text{ kg m}^{-3}$). The higher optical depth of the samples than in Gallet et al. (2009) might indicate a higher limit for the SSA measurements. Still, we included in the manuscript that SSA values above $60\text{ m}^2\text{ kg}^{-1}$

require caution. Out of a total of 4900 single measurements, SSA values above $60 \text{ m}^2 \text{ kg}^{-1}$ were recorded 499 times on 17 different days (10 %).

Changes in manuscript:

- 5 SSA values above $60 \text{ m}^2 \text{ kg}^{-1}$ require caution as the insufficient optical depth of the snow sample may cause artifacts as reported by Gallet et al. (2009). However, the densities of the snow samples for which Gallet et al. (2009) reported this limitation were below 100 kg m^{-3} , whereas the observed snow densities within this study were all well above this value (around 60 % of the samples with densities between $280\text{-}350 \text{ kg m}^{-3}$). The higher optical depth of the samples might indicate a higher limit for the SSA measurements. However, SSA values above $60 \text{ m}^2 \text{ kg}^{-1}$ occurred only in 10 % of the measurements..

P4 L15:

invert the temperatures

- 10 We followed your suggestion and changed it in the manuscript.

Fig 1:

I'm not convinced that this first figure (the octa plot) is useful for the paper. It shows raw data that are not used as is in the following and the interpretation is short and inconclusive. Instead, I suggest to plot a time-series (a normal one as for the air temperature, not a time versus date graph) cloudy/not cloudy as used by the algorithm to switch between diffuse/direct radiation.

- Thank you for your opinion and your suggestion for improvement. However, we think the hourly cloud cover plot is helpful to the reader in the way it is presented in the manuscript. Changing to a single time series of cloudy/cloudfree looks too crowded for the two months of measurements as cloudfree/cloudy periods partly switch too often. In the hourly plot, the times when measurements are analyzed can be identified much more precisely. We, therefore, added open and filled circles (corresponding to the same symbols used in Fig. 6) to the octa plot in order to both show the exact time of retrieval and whether the algorithm uses cloudless or overcast conditions. In that way, the cloud cover plot is much more meaningful compared to the original version. We adjusted the manuscript accordingly to account for the changes in Fig. 1.
- 15

Changes in manuscript:

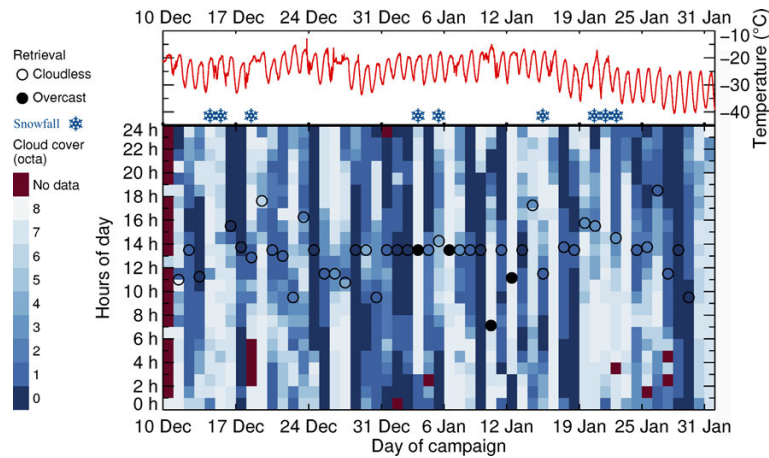


Figure 1. Time series of 2 m air temperature (red line) and hourly cloud cover (blueish squares) at Kohnen station between 10 December 2013 and 31 January 2014. Snowflake symbols denote days with snowfall. **Black circles show times when SSA was retrieved from CORAS measurements (Fig. 6) and denote retrievals for cloudless (open circles) and overcast (filled circles) conditions.**

3.2.1 Application in cloudless conditions

For each day, the times when SSA was retrieved from measurements with CORAS are added to Fig. 1 as black open circles. It has to be noted that the cloud cover was estimated from visual observation every full hour, whereas CORAS measurements were partly analyzed for times in between the visual observation and the cloud cover given here might not be representative for the actual CORAS measurement (e.g., 5 octa on 27 December 2013). Therefore, the CORAS measurements were carefully screened for any cloud contamination by analyzing the downward solar irradiance to guarantee homogeneous cloudless or overcast conditions.

3.2.2 Extension to overcast conditions

Retrievals in overcast conditions were applied on four days and are denoted as black filled circles in Fig. 1.

P5L1:

'polar day'. This term is ambiguous and the sentence is not strictly logical, air temperature decrease observed before the end of the 'polar day' is due to a change of solar elevation, not a change of day duration.

10 Thank you for pointing this out. We followed your suggestion and changed it in the manuscript.

Changes in manuscript:

Towards the end of the measurement period, the temperature level decreased due to **lower sun elevations**.

P5L10:

where these values of uncertainty are coming from ? As explained in the general comment, the description of the CORAS instrument and the evaluation of the uncertainty are missing. This part needs to be expanded but at least one paragraph. Please also consider the shadowing effect, frost formation, ... Information such as the cosine correction method, the frequency of observation, and other instrumental details are needed as well.

We carefully revised the uncertainty estimation and its description to make clear where the uncertainties of each measurement result from.

Changes in manuscript:

The spectral resolution is 2 to 3 nm between 0.3 and 1.0 μm and 15 nm up to 2.2 μm wavelength, **with a full spectrum measured every 15 s. The uncertainties of albedo measurements with CORAS range between 4.0 to 8.0 % depending on wavelength and combining different sources of instrumental errors. The signal-to-noise ratio accounts for 1.3-3.0 % uncertainty. Dark spectra were recorded constantly throughout the measurements resulting in a reliable correction for dark current and stray light within the spectrometer (0.1 % uncertainty). The wavelength calibration of the spectrometer accounts for 1.0 % uncertainty. For albedo measurements, the two optical inlets were cross-calibrated with an identical radiation source at four times during the observation period. The temporal stability of this cross-calibration is estimated with 1.0-4.5 % depending on wavelength. Furthermore, the non-ideal cosine characteristics of the irradiance optical inlets were characterized within the laboratory. The optical inlets were mounted on a turn table and the lamp signal under different angles of incidence (-95° to $+95^\circ$ in steps of 5°) was recorded. This procedure was repeated for four different relative azimuth angles between lamp and optical inlet and was used to compute correction factors for the cosine response depending on solar zenith angle, wavelength, and the direct fraction of the global irradiance. The azimuthal stability of the correction factors of 3.5 % was used to estimate the instrumental errors attributed to the non-ideal cosine response of the optical inlets. This way, the instrumental uncertainties combine to 6.8 % at 1280 nm wavelength. The analyzed measurement times were carefully selected to avoid errors due to frost formation and shadow effects which were typically observed during early morning.**

20 (...)

SMART **albedo** measurements have an estimated uncertainty between **4.1 to 8.1 %** also taking into consideration uncertainties due to the active horizontal stabilization of 1.0 %.

(...)

The measurement uncertainty of albedo measurements at 1280 nm wavelength was estimated with 6.8 %. Using \mathcal{R} , the uncertainty is reduced to 5.5 % as the transition to relative measurements yields independence from the cross-calibration. In addition to the instrumental errors, the surface slope at the footprint scale may influence the retrieval results. Using data from Picard et al. (2016), Dumont et al. (2017) found variations of the surface slope caused by wind drift at Dome C of $\pm 2^\circ$. They estimated a resulting uncertainty of 10 % in retrieved SSA due to these variations of the surface slope. Assuming a similar variability of the slope of the surface at Kohnen, an additional uncertainty of 10 % is assumed

for the retrieval of SSA. Applying Eq. 12 to the spectral albedo measured by CORAS on 24 December 2013 (Fig. 4a), the measured ratio \mathcal{R} of **0.702 ± 0.039** would lead to an estimated effective snow grain size of about **$90 \pm 31 \mu\text{m}$** at $\theta_0 = 54^\circ$ (blue and red lines in Fig. 4b). However, the relative uncertainty of the retrieval varies with solar position and effective snow grain size. In general, it is higher for smaller snow grains. Overall, the retrieval uncertainty ranges between **25 % and 37 %** for the

5 SSA throughout the measurement period.

(...)

The uncertainties of the retrieval were estimated similarly to the ground-based CORAS measurements, with the exception that the uncertainty of irradiance measurements is assumed to be slightly higher due to the remaining uncertainty in the horizontal leveling of the airborne sensors by the horizontal stabilization of SMART (**6.9 % at 1280 nm wavelength**). As a result, the

10 estimated uncertainty of the measured albedo ratio \mathcal{R} is about **5.6 %**.

P7L20:

Regarding the choice of the values of B and g in the 'middle of the range':

- 1) Values obtained from measurements are now available. Libois et al. 2013 and 2014 have measured B and recommended some values of g based on measurements.
- 2) The uncertainty of these values impacts the SSA estimation and needs to be taken into account in the evaluation of the uncertainties proposed in this paper which only considers instrumental uncertainties.

Thank you for this comment! Indeed, values of B and g based on measurements have been reported by Libois et al. The general recommendation by these authors is to refrain from spherical snow grains and use the shapes with $B=1.6 \pm 0.2$ to model snow grains. In our approach, we use $B=1.5$ which is in the range recommended by Libois et al. We are well aware that an inaccuracy in the particle form factor will affect the snow grain size retrieval. According to Zege et al. (2011), the retrieval inaccuracy

15 which may stem from the wrong assumption of A is less than 25 %. This has been highlighted in the text of the manuscript.

Changes in manuscript:

Within the SGSP algorithm, a value of 5.8 is used as an average value over a mixture of randomly oriented hexagonal plates and columns with $B(\xi) \approx 1.5$ and $g(\xi) \approx 0.84$. **This is in accordance with Libois et al. (2014) who recommend a value for $B(\xi)$ within 1.6 ± 0.2 based on measurements in Antarctica and the French Alps. Any inaccuracy in the form factor A**

20 **will affect the snow grain size retrieval in addition to instrumental errors. According to Zege et al. (2011), the retrieval inaccuracy which may stem from a false assumption of A is less than 25 %.**

P8L5-L8:

A few critical information are missing about the MODIS algorithm. - Which BRDF parameterization has been used and how ? - How the radiances have been converted to ground-level surface reflectances ? - Has an atmospheric model been used ? - Which product and version have been used here ?

The following clarifications are included into the manuscript:

1. MODIS Level 1B Collection 5 data have been used.

2. The angular reflective properties of the medium have been set via the particle form factor and the photon escape function. The BRDF is assumed to be wavelength independent.

5 3. The effect of the atmosphere has been removed using the radiative transfer model RAY (Tynes et al., 2011).

4. Subarctic winter atmospheric model (Kneizys et al., 1996) and Arctic background aerosol model (Tomasi et al., 2007) were used for constant atmospheric conditions. The amount of aerosol in Antarctica is in general two times less than in the Arctic (aerosol optical thickness 0.05 in the Arctic and 0.02-0.03 in the Antarctic at 500nm, from Tomasi et al. 2007 and AERONET data). The effect of this very low pollution onto the retrieval is considered to be negligible at the retrieval channels.

10

Changes in manuscript:

For the retrieval of effective snow grain size from satellite data, snow-atmosphere radiative interactions have to be taken into account by employing an atmosphere model as described in Zege et al. (2011). **The effect of the atmosphere has been removed employing the radiative transfer model RAY (Tynes et al., 2001) using the subarctic winter atmospheric model**
15 **(Kneizys et al., 1996) and the Arctic background aerosol model (Tomasi et al., 2007) for constant atmospheric conditions. The effect of the very low pollution in Antarctica (e.g., AOD of 0.015 at 500 nm at Kohnen station, Tomasi et al., 2007) onto the retrieval is considered to be negligible at the retrieval channels.**

Radiance data from MODIS (**Level 1B Collection 5**) onboard the Aqua and Terra satellites were used to retrieve effective snow grain sizes in the entire area covered by the campaign. The SGSP algorithm was applied for areas identified as
20 cloudless. After a preliminary separation of snow pixels, the effective snow grain size of each pixel is retrieved from radiance measurements of MODIS channels 3 (469 nm wavelength), 2 (858 nm), and 5 (1240 nm). **Assuming a spectrally constant bidirectional reflectance distribution function (BRDF) of snow and using the combination of three spectral channels, the angular dependency of the measured radiance is excluded.**

P9L13:

The argument implicitly assumes that the calibration error is wavelength-independent, which is often not the case. Even if the ratio R is less sensitive to calibration issues, the residual wavelength dependence can greatly affects the estimation of SSA as shown in Picard et al. 2016 (e.g. cosine correction, 100% direct assumption...).

We carefully revised the section on the measurement uncertainties and extended the description of the various sources of
25 uncertainty. For the changes made in the manuscript, please see the comment above.

P8L16:

these values have been obtained for perfect clear-sky. To my personal experience, direct/diffuse ratio shows huge variations in the infrared due to thin cloud (more than in the visible because the diffuse component is already quite large). Calculations of the atmosphere model with cloud with varying optical depth and crystal size would be useful, because the estimation of SSA using ratio (i.e. Eq 9) is sensitive to the spurious wavelength-dependence resulting from cloud cover.

It is true that thin clouds would change the direct/diffuse ratio significantly. We applied the retrieval under cloudless conditions using Eq. 9 only after a careful manual selection of the retrieval times based on a comparison between measured and simulated downward irradiance. Therefore, it was assured that no thin clouds did increase the diffuse radiation and contaminated the measurements and Eq. 3 is applicable. Nevertheless, also in cloudless conditions, the diffuse radiation is not zero. From radiative transfer simulations, we estimated the fraction of direct solar radiation with respect to the global irradiance to lie between 94.6 and 99.8 %. This value was used to quantify the retrieval uncertainties due to the assumption of 100 % direct radiation. However, we think a detailed sensitivity study with respect to cloud optical depth and crystal size would be beyond the scope of this study.

Changes in manuscript:

- 10 Hence, **after careful selection of cloudless periods**, the effective snow grain size can be calculated directly by inverting Eqs. 3 and 8.

P10L7:

I suggest to improve a little the justification of the constance of SSA during the day. E.g. doi:10.5194/tc-8-1205-2014

Thank you very much for pointing out this reference. Gallet et al. (2014) indeed found diurnal variations in SSA due to crystal growth in the same order of magnitude as observed from the CORAS retrieval. However, the changes observed by Gallet et al. strongly depend on meteorological conditions. Therefore, variations due to crystal growth can be not symmetric to noon and even change the sign on a day-to-day scale. Although an influence of crystal growth on the SSA variations cannot be ruled out for the measurements presented here, the evident dependence on the solar zenith angle and the symmetry to noon of the observed diurnal cycle of the SSA retrieved from CORAS strongly indicate that the crystal growth influences the results less than the changing solar zenith angle.

Changes in manuscript:

- 20 Furthermore, Gallet et al. (2014b) observed SSA variations on a sub-daily scale using the DUFISSS instrument (Dual Frequency Integrating Sphere for Snow SSA measurements; Gallet et al., 2009) at Dome C in January 2009. They measured a drop in SSA at around noon from $40 \text{ m}^2 \text{ kg}^{-1}$ to $33 \text{ m}^2 \text{ kg}^{-1}$ before the SSA increased again to $41 \text{ m}^2 \text{ kg}^{-1}$ at midnight. These temporal changes were attributed to the growth of sublimation crystals during daytime and nighttime formation of surface hoar. The SSA variations observed by CORAS on 24 December 2013 are in the same order of magnitude. However, the variations observed by Gallet et al. (2014b) are not symmetric to noon and their sign changes on a day-to-day scale due to the strong dependence on meteorological conditions. Even though an influence of crystal growth

processes cannot be ruled out for the measurements presented here, the evident dependence on the solar zenith angle and the constant symmetry to noon of the diurnal cycle observed in the SSA retrieved from CORAS measurements strongly indicate a dominating influence of the solar zenith angle.

P10L10:

the surface roughness/slope at the footprint scale is another likely player that affects the theory used here. See e.g. Dumont et al. 2017 in TC (see the slope estimation).

Thank you for pointing at this specific reference. We included a discussion on the uncertainties introduced by the unknown
5 slope at the footprint scale (see comment above).

P14L5:

the argument on the scales seems weak because the airborne data are between the in-situ and MODIS data in terms of scales and MODIS shows little bias w/r to in-situ measurements. I guess that the authors have analyzed in details the spectra and various sources of errors from the different sensors without success. May be add part of this analysis. For instance, showing coincident spectra from the different sensors could help to understand the differences, and at least to rule out some potential defects of the sensors.

It is true that the airborne data are between the in situ and MODIS data in terms of scales. However, whereas MODIS averages over $50 \times 50 \text{ km}^2$ with Kohnen station situated in the central pixel, the area over which the airborne data is averaged is largely determined by the flight track. Thereby, local influences on the SSA cannot be ruled out entirely. Furthermore, unidentified systematical errors in the airborne SMART measurements are a possible reason for the underestimation of SSA and deserve
10 further attention in future studies. We further clarified that within the manuscript.

Changes in manuscript:

SMART measurements have a larger footprint and were averaged over an area of $5 \times 5 \text{ km}^2$ surrounding Kohnen station.

Furthermore, the area over which the airborne data is averaged is largely determined by the flight track. On such scales, the local small-scale variability of SSA as indicated by the in situ measurements can lead to significant differences in
15 SSA. Already along the 100 m-transect, in situ SSA varied by up to 34 % (4 January 2014). On larger scales, this variability is likely to increase. **In addition, unidentified systematical errors in the airborne SMART measurements are a possible reason for the underestimation of SSA and deserve further attention in future studies.**



Comparison of different methods to retrieve effective snow grain size in central Antarctica

Tim Carlsen¹, Gerit Birnbaum², André Ehrlich¹, Johannes Freitag², Georg Heygster³, Larysa Istomina³, Sepp Kipfstuhl², Anaïs Orsi⁴, Michael Schäfer¹, and Manfred Wendisch¹

¹Leipzig Institute for Meteorology, Leipzig University, Leipzig, Germany

²Alfred Wegener Institute, Helmholtz Centre for Polar and Marine Research, Bremerhaven, Germany

³Institute of Environmental Physics, University of Bremen, Bremen, Germany


⁴Laboratoire des Sciences du Climat et de l'Environnement, Gif-sur-Yvette, France

Correspondence to: Tim Carlsen (tim.carlsen@uni-leipzig.de)

Abstract. The effective size of snow grains (r_{eff}) affects the reflectivity of snow surfaces and ~~thus~~, thus, the local surface energy budget in particular in polar regions. Therefore, the specific surface area (SSA) was monitored as an equivalent measure for snow grain size was observed for a two-month period in central Antarctica (Kohnen research station) during austral summer 2013/14. The data were retrieved on the basis of ground-based spectral surface albedo measurements collected by the Compact Radiation measurement System (CORAS; ~~ground-based~~ and and airborne observations with the Spectral Modular Airborne Radiation measurement system (SMART; ~~airborne~~). The Snow Grain Size and Pollution amount (SGSP) algorithm, originally developed to analyze spaceborne reflectance measurements by the MODerate Resolution Imaging Spectroradiometer (MODIS), was modified ~~and applied to the ground-based and airborne observations collected in this study. Furthermore, spectral in order to reduce the impact of the solar zenith angle on the retrieval results and to cover measurements in overcast conditions. Spectral~~ ratios of surface albedo at 1280 nm and 1100 nm wavelength were used to reduce the retrieval uncertainty. ~~Additionally, the algorithm originally developed for cloudless conditions was adapted to handle overcast conditions. Optical~~ The retrieval was applied to the ground-based and airborne observations and validated against optical in situ observations of SSA utilizing an IceCube device ~~were used to validate the retrieval results~~. The SSA retrieved from CORAS observations varied between $27 \text{ m}^2 \text{ kg}^{-1}$ and ~~8689~~ $869 \text{ m}^2 \text{ kg}^{-1}$. Snowfall events caused distinct ~~SSA maxima which were often relative maxima of the SSA which were~~ followed by a gradual decrease in SSA due to snow metamorphism and wind-induced transport of fresh fallen ice crystals (~~vice versa for r_{eff}~~). ~~SSA retrieved by data from~~. The ability of the modified algorithm to include measurements in overcast conditions improved the data coverage especially at times when precipitation events occurred and the SSA changed quickly. SSA retrieved from measurements with CORAS and MODIS agree with the in situ observations within the ranges given by the measurement uncertainties. However, SSA retrieved ~~by from~~ the airborne SMART ~~observations data~~ underestimated the ground-based ~~observations results~~ by a factor of ~~2.1 (overestimation of r_{eff})~~ 2.

1 Introduction

The cryosphere plays a fundamental role in determining the Earth's surface radiative energy budget, as snow and sea ice represent surfaces with the highest albedo on Earth. Picard et al. (2016) estimated that a hypothetical change in global surface albedo of one percent would ~~result in offset~~ a difference in reflected energy comparable to the globally averaged radiative forcing of 1.82 W m^{-2} caused by the increase in CO_2 concentration since the preindustrial time (Myhre et al., 2013). This change in global surface albedo could be caused either by a variation in snow and sea ice cover or by a change of the snow albedo itself. During boreal winter, snow and sea ice cover up to 15 % of the Earth's surface (Vaughan et al., 2013). Although these areas are mainly in polar regions with ~~mostly low~~ partly low values of incoming solar radiation, the high ~~values of~~ snow and sea ice albedo may facilitate substantial changes in the local surface energy budget. In Antarctica, more than 99.8 % of the continent (~~Burton-Johnson et al., 2016~~) and most of the sea ice are covered with snow ~~with little seasonal variability~~ all year round (~~Burton-Johnson et al., 2016~~). However, the snow surface albedo varies both on ~~a~~-temporal and spatial ~~scales~~ scales. For example, Munneke et al. (2008) found variations of the broadband albedo of snow ~~at five different locations in Dronning Maud Land~~ in a range between 0.77 and 0.88 at five locations in Dronning Maud Land.

~~This variability is~~ Changes of broadband and spectral snow albedo are caused by different parameters such as snow grain size (and shape), surface roughness (e.g., Warren et al., 1998), soot content (e.g., Bond et al., 2013), and cloudiness; ~~it~~. It further depends on wavelength (e.g., Hudson et al., 2006; Warren and Brandt, 2008) ~~and as well as~~ solar position (e.g., Wiscombe and Warren, 1980; Wiscombe, 1980; Dumont et al., 2010). ~~Furthermore, snow surface albedo, and~~ varies with snow depth ~~and the~~ (e.g., Wiscombe and Warren, 1980) ~~and~~ liquid water content. ~~Out of~~ (e.g., Wiscombe and Warren, 1980; Gallet et al., 2014a). From these parameters, the snow grain size has the largest effect on snow albedo. ~~Measurements on the East Antarctic plateau show that an increase in~~ Simulations by Wiscombe and Warren (1980) showed that the spectral albedo in the near-infrared part of the spectrum may drop by a factor of 2 or more when the snow grain size ~~due to snow metamorphism may decrease the local surface albedo by three percent~~ (Freitag et al., in prep.) increases from $50 \mu\text{m}$ to $1000 \mu\text{m}$. Dang et al. (2015) showed that the transition from fresh fallen snow with a typical  effective snow grain size of $100 \mu\text{m}$ to ~~old aged~~ snow ($1000 \mu\text{m}$) leads to a decrease in ~~solar~~ snow albedo (spectrally integrated over $0.3\text{--}4.0 \mu\text{m}$) of 15 % from 0.83 to 0.72. This relation could clearly ~~be identified in ground-based measurements by Domine et al. (2006) analyzing snow samples taken at Svalbard in 2001. They measured a decrease in reflectance at 1310 nm wavelength by 45 % with increasing grain size from $290 \mu\text{m}$ to $1175 \mu\text{m}$. Libois et al. (2015) and Picard et al. (2016) retrieved a three-year time series of SSA from spectral albedo measurements at Dome C ($75^\circ 6' \text{ S}$, $123^\circ 0' \text{ E}$), Antarctica, which emphasized the dynamical evolution of near-surface SSA by displaying a 3-fold decrease every summer in response to the increase of air temperature. A detailed comparison of this dataset with snow model simulations and a geophysical interpretation are presented by Libois et al. (2015). Similar seasonal variations but little year-to-year variation was found by Jin et al. (2008) who retrieved snow grain size from measurements with the MODerate Resolution Imaging Spectroradiometer (MODIS) at 1.64 and $0.64 \mu\text{m}$ wavelength over the Antarctic continent for four days each year between 2000 and 2005. Therefore, a positive feedback mechanism can be postulated: increasing snow temperatures are followed by an accelerated snow metamorphism and a decrease of the snow albedo, which leads to higher absorption~~

and heating of the snow. However, the expected snow albedo decrease due to temperature-induced metamorphism (0.3 % for a warming of 3 K) can be overcompensated by an increase in snow albedo by 0.4 % owing to a projected increase in precipitation during the twenty-first century in interior Antarctica (Picard et al., 2012).

5 The larger the snow grains are, the longer is the photon path length through the individual ice crystals and the higher is the probability of photon absorption leading to a lower surface albedo (Wiscombe and Warren, 1980). This effect is most pronounced at wavelengths larger than 1000 nm where the imaginary part of the complex refractive index of ice increases. Observations showed that the ~~grain size~~ geometric grain size (from visual determination) of snow crystals varies between 10 μm for fresh fallen snow and up to 3 mm for ~~old aged~~ snow (Fierz et al., 2001). As snow ages, the grains become larger and more spherical (Colbeck, 1983; Kaempfer and Schneebeli, 2007). This snow metamorphism can even be effective at temperatures below the freezing ~~level~~ temperature and is influenced by the vertical temperature profile within the snowpack, the snow structure, air temperature, and air humidity.

10 The grain size is traditionally defined by the ~~geometric~~ geometric length of the largest extension of a snow grain (Fierz et al., 2009; Leppänen et al., 2015), which ~~may cause~~ causes ambiguities due to the complex shapes of snow grains. Therefore, not only for radiative transfer applications, the optical-equivalent grain size is introduced as the effective radius r_{eff} of a collection of spheres with the same volume-to-surface ratio compared to the actual non-spherical snow grains (Grenfell and Warren, 1999; Neshyba et al., 2003). The specific surface area (SSA, surface area of ice-air interface per unit mass) is related to the optical-equivalent grain size effective radius of the snow grains and the density of ice ρ_{ice} (917 kg m^{-3}) by:

$$\text{SSA} = \frac{3}{\rho_{\text{ice}} \cdot r_{\text{eff}}}. \quad (1)$$

SSA (in units of $\text{m}^2 \text{ kg}^{-1}$) ~~can be measured with different~~ is measured with techniques such as methane adsorption (e.g., Domine et al., 2001; Legagneux et al., 2002), stereology (e.g., Matzl and Schneebeli, 2010), and X-ray microtomography (e.g., Flin et al., 2005; Kaempfer and Schneebeli, 2007). Those methods are difficult to employ in the field. Therefore, optical measurements that utilize the spectral absorption of snow grains are applied in field studies (e.g., Gallet et al., 2009) for the in situ measurement of SSA. However, in situ techniques to measure SSA are restricted to single observation sites. Consequently, longer time series of SSA are scarce in remote Arctic and Antarctic areas.

25 To retrieve SSA and r_{eff} , measurements of reflected solar radiation are required (e.g., Bohren and Barkstrom, 1974; Wiscombe, 1980; Grenfell et al., 1994). The retrievals ~~use these radiation measurements and~~ are based on the spectral variability of snow albedo as a function of effective snow grain size. Snow albedo models are ~~used~~ employed to calculate the spectral albedo and to invert the measurements to retrieve the effective snow grain size (e.g., Wiscombe and Warren, 1980). These albedo models mostly assume spherical grains, which is ~~critical~~ unrealistic because the grain shape is usually far from being spherical. ~~As shown by Dang et al. (2016), the representation of~~ (e.g., Kokhanovsky and Zege, 2004; Libois et al., 2013; Leppänen et al., 2015). Picard et al. (2009) estimated an uncertainty of $\pm 20\%$ when determining SSA from albedo measurements in case of an unknown snow grain shape. A common approach to account for the non-spherical shape of snow grains is to represent the non-spherical snow grains by a population of spherical grains with the same area-to-mass ratio in the spectral albedo model.

However, as shown by Dang et al. (2016), this approximation can lead to an underestimation of the retrieved effective snow grain size by a factor of 2.4, more than 2.

Several algorithms have been developed that consider snow grains of irregular shape (e.g., Kokhanovsky and Zege, 2004; Lyapustin et al., 2009). The Snow Grain Size and Pollution amount (SGSP) retrieval algorithm by Zege et al. (2011) to analyze satellite observations by the ~~MODerate-Resolution-Imaging-Spectroradiometer (MODIS)~~ MODIS was validated against ground-based in situ measurements from the Arctic, the Antarctic, Greenland, and Japan revealing a correlation coefficient of 0.86 (Wiebe et al., 2013). However, Up to now, grain size products of polar orbiting satellites do not provide a sufficiently high temporal resolution that may resolve snow precipitation events and snow and metamorphism that typically can advance in a matter of hours.

In this study, ground-based measurements with high temporal resolution were utilized to study the evolution of effective snow grain size in central Antarctica. Independent methods are introduced and applied in Sect. 2. The SGSP retrieval algorithm was further developed advanced and adapted to ground-based spectral albedo measurements as discussed in Sect. 3. The obtained resulting time series of effective snow grain size estimates is presented in Sect. 4 including results from in situ measurements (Freitag et al., in prep.) as well as from remote sensing by ground-based and additional airborne and satellite observations.

2 Measurements and instrumentation

The measurements were conducted at and in the vicinity of the Kohnen research station operated by the Alfred Wegener Institute, Helmholtz Centre for Polar and Marine Research (AWI). Kohnen station is located at the outer part of the East Antarctic plateau (75° 0' S, 0° 4' E, 2892 m a.s.l. above sea level), approximately 500 km from the coastline, where the local weather and climate is mostly determined by weak catabatic winds. The annual snow accumulation is 62 mm liquid water equivalent (Oerter et al., 2000) with moderate snowfall (1 mm to more than 5 mm water equivalent) occurring only a few times per year (Birnbaum et al., 2006). The atmosphere is both clean with an Aerosol Optical Depth (AOD) at Kohnen station of 0.015 (at 500 nm, measured 2001-2006, Tomasi et al., 2007) and dry (mean integrated atmospheric water vapor between December 2013 and January 2014: 1.1 kg m⁻²). The black carbon (BC) load-concentration in the snowpack on the Antarctic plateau is low; for the South Pole, Hansen and Nazarenko (2004) reported a mean BC load-concentration of 0.2 ppbw (parts per billion by weight).

2.1 Ground-based observations

The ground-based measurements were embedded in the 'Coldest Firn' (CoFi) project by AWI, which targets investigates microstructure as well as physical and chemical composition of snow and firn on the Antarctic plateau. Solar broadband and spectral radiation measurements of snow surface albedo combined with meteorological observations (temperature, humidity, wind velocity and direction, radio sounding, synoptic observations) were conducted. In addition, effective snow grain size and density of snow samples were measured in situ on a daily basis at Kohnen station, accompanied by measurements of vertical snow temperature profiles (Freitag et al., in prep.). Snow samples from in situ measurements were extracted daily (ex-

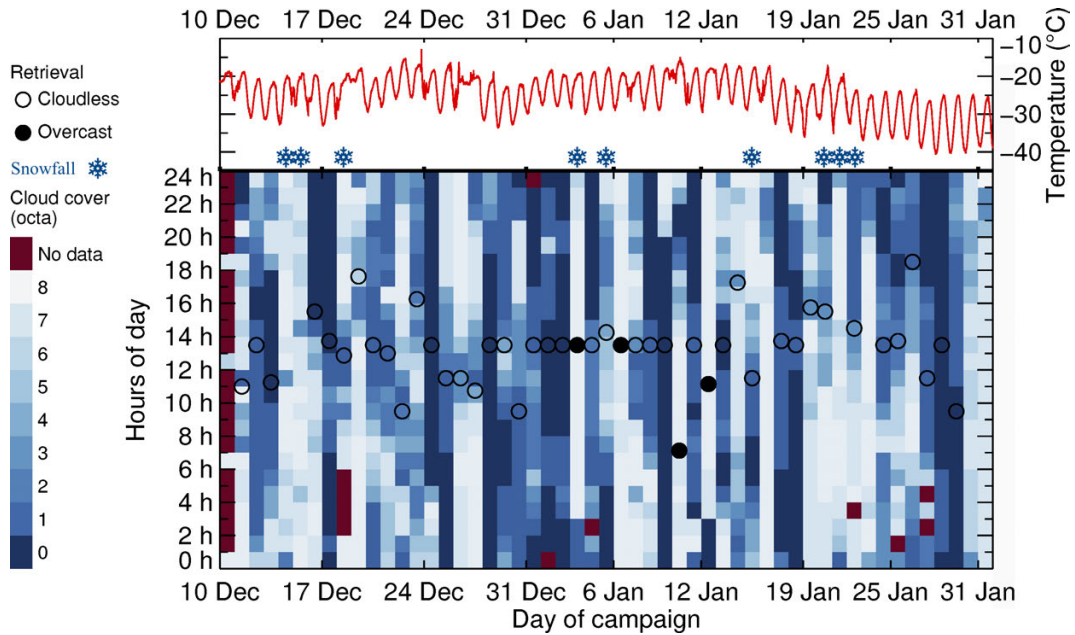


Figure 1. Time series of 2 m air temperature (red line) and hourly cloud cover (blueish squares) at Kohnen station between 10 December 2013 and 31 January 2014. Snowflake symbols denote days with snowfall. [Black circles show times when SSA was retrieved from CORAS measurements \(Fig. 6\) and denote retrievals for cloudless \(open circles\) and overcast \(filled circles\) conditions.](#)

cept on 5 December, 12, 17, 18, and 19 January) along a 100 m-transect. After extraction, the measurements of SSA were conducted with an IceCube device, which uses a laser diode at 1310 nm to illuminate the snow sample underneath an integrating sphere (Gallet et al., 2009). The reflected signal is detected by a photodiode. By means of a certified standard, the hemispherical infrared reflectance is derived, which is used to calculate SSA and r_{eff} applying a radiative transfer model (for details, see Gallet et al., 2009). For the derived SSA values between 5 to $130 \text{ m}^2 \text{ kg}^{-1}$, the measurement uncertainty is in the range of 10 % (Freitag et al., in prep.). SSA values above $60 \text{ m}^2 \text{ kg}^{-1}$ require caution as the insufficient optical depth of the snow sample may cause artifacts as reported by Gallet et al. (2009). However, the densities of the snow samples for which Gallet et al. (2009) reported this limitation were below 100 kg m^{-3} , whereas the observed snow densities within this study were all well above this value (around 60 % of the samples with densities between $280\text{--}350 \text{ kg m}^{-3}$). The higher optical depth of the samples might indicate a higher limit for the SSA measurements. However, SSA values above $60 \text{ m}^2 \text{ kg}^{-1}$ occurred only in 10 % of the measurements.

Two downward-looking digital cameras were employed for ground-based photogrammetric measurements of surface roughness structures. Another digital camera was used to resolve the hemispherical-directional reflectance factor (HDRF) of the snow surface following a method described by Ehrlich et al. (2012). For the definition of reflectance quantities used within this study, we refer to Schaepman-Strub et al. (2006). Furthermore, an all-sky camera was used for cloud observations. AOD was determined by means of a sun photometer.

The ground-based measurements were carried out during austral summer between 4 December 2013 and 31 January 2014. Within this period, nine snowfall events occurred (recorded by visual observation), surface temperature ranged from ~~-15-40~~ °C to ~~-40-15~~ °C. The time series of the measured 2 m air temperature and the hourly cloud fraction are presented in Fig. 1. The temperature indicates diurnal cycles on most days. Only on days with high cloud cover almost constant air temperatures were observed. Towards the end of the measurement period, the temperature level decreased due to ~~the approaching end of the polar day~~ lower sun elevations. The mean total cloud amount over the entire period was less than 4 octa. Only five completely overcast days were reported. ~~Total~~ The total cloud cover was highly variable and mainly influenced by cirrus clouds.

The spectral snow albedo $\alpha(\lambda)$ was measured from ~~both~~ ground-based and airborne instruments. At Kohnen station, the COmpact RAdiation measurement System (CORAS) measured upward and downward spectral irradiance [$F^\uparrow(\lambda)$, $F^\downarrow(\lambda)$] within 0.3 to 2.2 μm wavelength. The spectral snow albedo was obtained by:

$$\alpha(\lambda) = \frac{F^\uparrow(\lambda)}{F^\downarrow(\lambda)}. \quad (2)$$

The spectral resolution is 2 to 3 nm between 0.3 and 1.0 μm and 15 nm up to 2.2 μm wavelength. ~~The uncertainty, with a full spectrum measured every 15 s. The uncertainties of albedo measurements with CORAS of 3.3 range between 4.0 to 8.0 % depending on wavelength and combining different sources of instrumental errors. The signal-to-noise ratio accounts for 1.3-3.0 % combines the uncertainties associated with the radiometric calibration using an integrating sphere (1.4 uncertainty.~~ Dark spectra were recorded constantly throughout the measurements resulting in a reliable correction for dark current and stray light within the spectrometer (0.1 %), ~~the signal-to-noise ratio, dark current, and uncertainty~~. The wavelength calibration of the spectrometer ~~(2.5 accounts for 1.0 %) as well as the correction of uncertainty.~~ For albedo measurements, the two optical inlets were cross-calibrated with an identical radiation source at four times during the observation period. The temporal stability of this cross-calibration is estimated with 1.0-4.5 % depending on wavelength. Furthermore, the non-ideal cosine ~~characteristic~~ characteristics of the irradiance optical inlets ~~(1.0 were characterized within the laboratory. The optical inlets were mounted on a turn table and the lamp signal under different angles of incidence (-95° to +95° in steps of 5°) was recorded. This procedure was repeated for four different relative azimuth angles between lamp and optical inlet and was used to compute correction factors for the cosine response depending on solar zenith angle, wavelength, and the direct fraction of the global irradiance. The azimuthal stability of the correction factors of 3.5 %) was used to estimate the instrumental errors attributed to the non-ideal cosine response of the optical inlets. This way, the instrumental uncertainties combine to 6.8 % at 1280 nm wavelength. The analyzed measurement times were carefully selected to avoid errors due to frost formation and shadow effects which were typically observed during early morning.~~

The location and mounting of the ground-based instrumentation are illustrated in Fig. 2. Table 1 lists the ground-based and airborne instruments relevant to investigate the evolution of snow microphysical and optical properties.

2.2 Airborne data

To characterize the representativeness of the local ground-based observations, an intensive observation phase including airborne measurements using the Polar 6 research aircraft from AWI was conducted between 24 December 2013 and 5 January 2014.

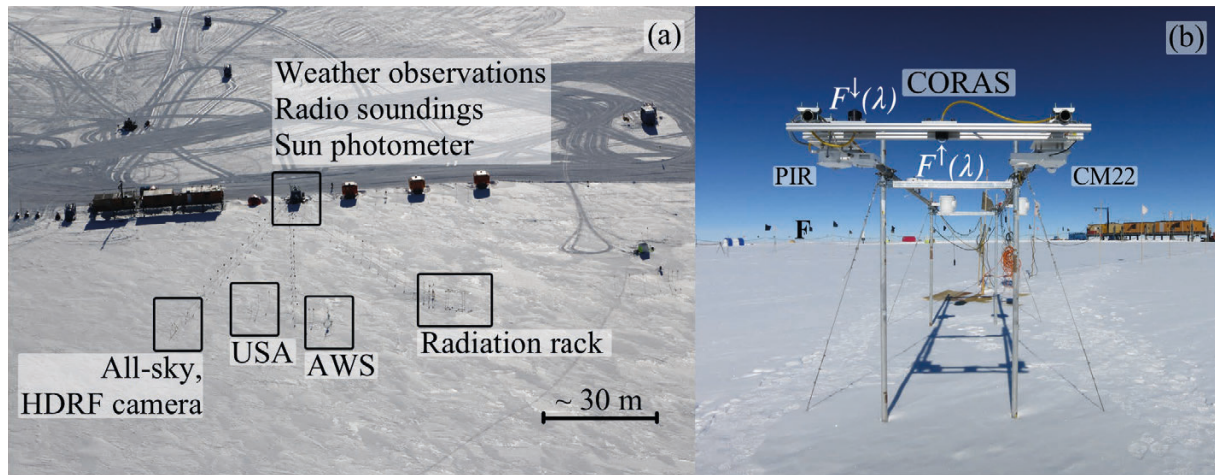


Figure 2. Left (a): Aerial photograph of Kohnen station. The positions of different ground-based instruments are marked with black rectangles. USA: Ultrasonic anemometer. AWS: Automatic weather station. Right (b): Instrument setup at the ground-based radiation rack: optical inlets of the CORAS instrument and the broadband radiation instruments CM22 and PIR.

The aircraft flew 60 hours to characterize the spatial variability of snow properties above Dronning Maud Land. A map of the tracks of the 18 research flights is shown in Fig. 3. During each flight, an overpass over Kohnen station was realized to compare airborne and ground-based measurements. The airborne observations covered a wide variety of surface roughness structures as well as ~~different~~ precipitation patterns, which strongly influence snow albedo. Beside solar broadband and spectral radiation measurements, the airborne observations included measurements of snow HDRF by means of a digital camera and surface roughness measurements using a laser scanner. Meteorological measurements were provided by the Aircraft-Integrated Meteorological Measurement System (AIMMS20). The aircraft instrumentation additionally included geophysical observations within the CoFi project (snow and ice thickness).

On Polar 6, irradiance measurements similar to the ground-based observations were conducted using the Spectral Modular Airborne Radiation measurement sysTem (SMART) which applies an active horizontal stabilization of the optical inlets to correct for aircraft movement (Wendisch et al., 2001; Ehrlich et al., 2008). SMART albedo measurements have an estimated uncertainty ~~of 3.4~~ between 4.1 to 8.1 % also taking into consideration ~~an additional source of uncertainty~~ uncertainties due to the active horizontal stabilization of 1.0 %.

3 Methodology

3.1 SGSP retrieval algorithm using satellite data

Absorption of solar radiation by ice ~~gets~~ becomes crucial in the near-infrared part of the solar wavelength spectrum (Warren and Brandt, 2008). As the effective photon path is longer within larger snow grains, the magnitude of absorption is determined

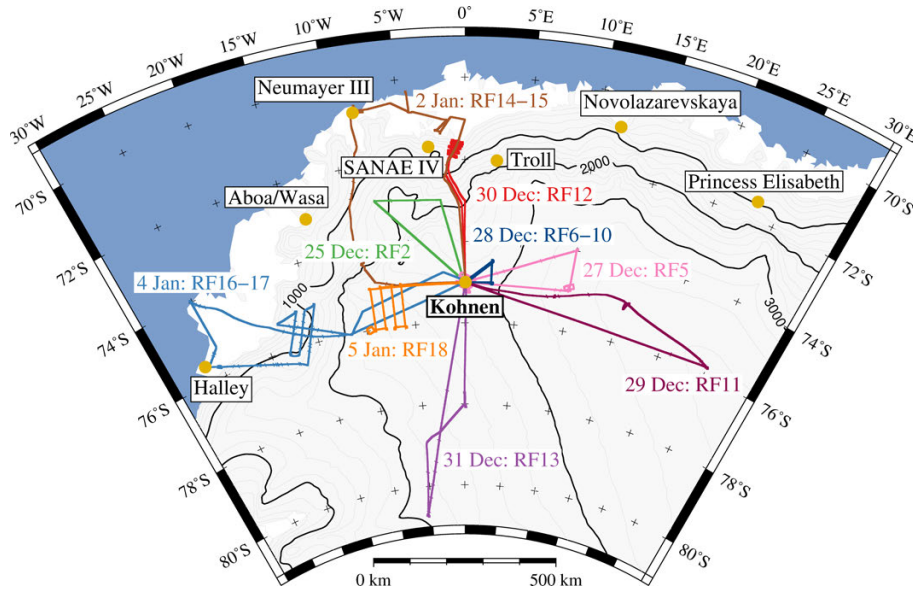


Figure 3. Map of flight patterns with the Polar 6 research aircraft during the campaign. Each color corresponds to a different flight.

by the size of the snow grains. Hence, snow surface albedo in the near-infrared mainly depends on the effective snow grain size. Zege et al. (1991) showed that the plane albedo $\alpha_p(\theta_0)$ as a function of solar zenith angle θ_0 can be parameterized using an asymptotic solution of the radiative transfer theory by:

$$\alpha_p(\theta_0) = \exp[-y \cdot K_0(\theta_0)] \quad \text{with} \quad K_0(\theta_0) = \frac{3}{7} (1 + 2 \cos \theta_0).$$

5

$$\alpha_p(\theta_0) = \exp[-y \cdot K_0(\theta_0)], \quad \text{with} \quad (3)$$

$$K_0(\theta_0) = \frac{3}{7} (1 + 2 \cos \theta_0). \quad (4)$$

The escape function $K_0(\theta_0)$ (dimensionless) describes the angular distribution of the number of photons escaping from a non-absorbing, semi-infinite medium. The uncertainty introduced by its approximation of α_p introduced by the approximation of $K_0(\theta_0)$ given in Eq. 3-4 (Kokhanovsky and Zege, 2004) is below 2 % for $\theta_0 < 78^\circ$. Following Kokhanovsky and Zege (2004), the parameter y depends on the volumetric extinction and absorption coefficients of snow b_{ext} and b_{abs} (both in m^{-1}) and the dimensionless asymmetry parameter (average cosine over the phase function) $g(\xi)$ of the snow grain which shape is represented by the parameter ξ :

$$y = 4 \sqrt{\frac{b_{\text{abs}}}{3 b_{\text{ext}} \cdot [1 - g(\xi)]}}. \quad (5)$$

Assuming pure snow and applying the [framework principles](#) of geometrical optics, the volumetric extinction and absorption coefficients of snow can be derived by (Kokhanovsky and Zege, 2004):

$$\underline{b_{\text{ext}} = \frac{1.5 C_v}{r_{\text{eff}}} \quad \text{and} \quad b_{\text{abs}} = B(\xi) \cdot b_{\text{abs,ice}} \cdot C_v = B(\xi) \cdot \frac{4\pi \chi}{\lambda} \cdot C_v,}$$

~~and~~

$$5 \quad \underline{b_{\text{ext}} = \frac{1.5 C_v}{r_{\text{eff}}}, \quad \text{and}} \tag{6}$$

$$\underline{b_{\text{abs}} = B(\xi) \cdot b_{\text{abs,ice}} \cdot C_v = B(\xi) \cdot \frac{4\pi \chi}{\lambda} \cdot C_v.} \tag{7}$$

[b_{ext} and b_{abs}](#) only depend on the volumetric concentration of snow grains C_v (dimensionless, $\rho_{\text{snow}}/\rho_{\text{ice}}$), the effective snow grain size r_{eff} , the absorption enhancement parameter $B(\xi)$ (dimensionless), and the absorption coefficient of pure ice $b_{\text{abs,ice}}$ (m^{-1}), which is determined by the imaginary part of the complex refractive index of ice χ at wavelength λ . Consequently, Eq.

10 5 reduces to:

$$\underline{y = A \cdot \sqrt{\frac{4\pi \chi}{\lambda} \cdot r_{\text{eff}}} \quad \text{with} \quad A = \frac{4}{3} \sqrt{\frac{2B(\xi)}{1-g(\xi)}}.}$$

$$\underline{y = A \cdot \sqrt{\frac{4\pi \chi}{\lambda} \cdot r_{\text{eff}}}, \quad \text{with}} \tag{8}$$

$$\underline{A = \frac{4}{3} \sqrt{\frac{2B(\xi)}{1-g(\xi)}}.} \tag{9}$$

15 The form factor A accounts for the snow grain shape ~~only~~ by merging $B(\xi)$ and $g(\xi)$ into a single parameter. Equation 8 forms the basis of the SGSP retrieval algorithm by Zege et al. (2011) who applied the χ data base by Warren and Brandt (2008) and assumed a form factor of $A = 5.8$. The factor A varies in general between 5.1 (Kokhanovsky and Macke, 1997) for fractals and 6.5 for spheres. Within the SGSP algorithm, a value of 5.8 is used as an average value over a mixture of randomly oriented hexagonal plates and columns with $B(\xi) \approx 1.5$ and $g(\xi) \approx 0.84$. [This is in accordance with Libois et al. \(2014\) who](#)

20 [recommend a value for \$B\(\xi\)\$ within \$1.6 \pm 0.2\$ based on measurements in Antarctica and the French Alps. Any inaccuracy in the form factor \$A\$ will affect the snow grain size retrieval in addition to instrumental errors. According to Zege et al. \(2011\), the retrieval inaccuracy which may stem from a false assumption of \$A\$ is less than 25 %.](#) For the retrieval of effective snow grain size from satellite data, snow-atmosphere radiative interactions have to be taken into account by employing an atmosphere model as described in Zege et al. (2011). [The effect of the atmosphere has been removed employing the radiative transfer](#)

25 [model RAY \(Tynes et al., 2001\) using the subarctic winter atmospheric model \(Kneizys et al., 1996\) and the Arctic background aerosol model \(Tomasi et al., 2007\) for constant atmospheric conditions. The effect of the very low pollution in Antarctica \(e.g., AOD of 0.015 at 500 nm at Kohnen station, Tomasi et al., 2007\) onto the retrieval is considered to be negligible at the retrieval channels.](#)

Radiance data from MODIS ([Level 1B Collection 5](#)) onboard the Aqua and Terra satellites were used to retrieve effective snow grain sizes in the ~~entire~~-area covered by the campaign. The SGSP algorithm was applied for areas identified as cloudless. After a preliminary separation of snow pixels, the effective snow grain size of each pixel is retrieved from radiance measurements of MODIS channels 3 (469 nm wavelength), 2 (858 nm), and 5 (1240 nm). [Assuming a spectrally constant bidirectional reflectance distribution function \(BRDF\) of snow and using the combination of three spectral channels, the angular dependency of the measured radiance is excluded.](#)

The final product of estimated effective [snow](#) grain sizes is provided in 2D-maps of spatial resolution of 1 km. For the local effective snow grain size at Kohnen station, the spatial average of the 50 x 50 pixel of MODIS surrounding the geographic coordinates of Kohnen was calculated. Daily averages combine up to four MODIS overpasses per day under cloudless conditions.

For the solar zenith angle range between 60° and 80°, the relative error of the retrieval is below 10 % for effective [snow](#) grain sizes between 30 μm to 300 μm. It grows with increasing solar zenith angle and gets as high as 20 % for $\theta_0 = 85^\circ$, and even higher for lower sun elevations. Therefore, the retrieval is generally not applied for $\theta_0 > 85^\circ$. The large uncertainty of the SGSP retrieval for high solar zenith angles is related to the ~~conversion of the measured reflectance from one viewing direction by the satellite sensor into measured albedo. For this, the bidirectional reflectance distribution function (BRDF) of the snow surface has to be assumed. Due to assumptions on the particle form factor A and the approximation of the escape function $K_0(\theta_0)$ which is less accurate for oblique illumination angles. In combination with~~ the strong forward scattering characteristic for snow grains, small errors in the assumed ~~BRDF A and $K_0(\theta_0)$ can~~ greatly distort the albedo, ~~especially at low sun elevations. Similarly, the spectral behavior of the BRDF of snow slightly depends on the illumination angle (Zege et al., 2011).~~ Consequently, within this work the satellite retrieval is limited to $\theta_0 \leq 75^\circ$. Furthermore, an additional uncertainty of 2 % originates from the atmospheric model.

3.2 Retrieval of effective snow grain size from spectral albedo measurements

In contrast to the satellite observations, for the ground-based and airborne spectral albedo measurements, the atmospheric influence can be neglected because of the high surface elevation providing a dry and aerosol-free atmosphere (Wendisch et al., 2004). To test this assumption, the direct fraction of global irradiance was simulated with the library for radiative transfer libRadtran by Mayer and Kylling (2005) using the discrete ordinate radiative transfer solver DISORT by Stamnes et al. (1988). The radiosondes released up to four times a day were used for meteorological input (profiles of air temperature, relative humidity, and static air pressure). The contribution of direct solar radiation to the global irradiance measured at the surface was estimated to vary between 94.6 and 99.8 % at the wavelengths used in the retrieval algorithm. Therefore, the simulated diffuse part hardly exceeded 5 % of the total incident irradiance. Hence, [after careful selection of cloudless periods](#), the effective snow grain size can be calculated directly by inverting Eqs. 3 and 8:

$$r_{\text{eff}} = \left[\frac{\ln \alpha_p}{A \cdot K_0(\theta_0) \cdot \sqrt{\frac{4\pi X}{\lambda}}} \right]^2. \quad (10)$$

The uncertainty of the retrieved r_{eff} is related to the measured albedo and the assumed particle shape. Especially surface albedo values close to unity are uncertain due to the small differences between upward and downward irradiance. To minimize uncertainties, the retrieval algorithm was adapted to spectral ratio measurements as introduced by Werner et al. (2013) and Brückner et al. (2014). Using ratios of measured snow albedo at different wavelengths decreases the retrieval error as the impact of measurement uncertainties is reduced. For the ground-based CORAS and airborne SMART measurements, the ratio \mathcal{R} of albedo measurements at 1280 nm normalized by the albedo at a weakly absorbing wavelength of 1100 nm was used:

$$\mathcal{R} = \frac{\alpha(\lambda_1 = 1280 \text{ nm})}{\alpha(\lambda_2 = 1100 \text{ nm})}. \quad (11)$$

Equation 10 thus changes to:

$$r_{\text{eff}} = \left\{ \frac{\ln \mathcal{R}}{A \cdot K_0(\theta_0) \cdot \left[\sqrt{\frac{4\pi \chi(\lambda_2)}{\lambda_2}} - \sqrt{\frac{4\pi \chi(\lambda_1)}{\lambda_1}} \right]} \right\}^2 \quad \text{with } \lambda_1 = 1280 \text{ and } \lambda_2 = 1100. \quad (12)$$

10 with $\lambda_1 = 1280 \text{ nm}$ and $\lambda_2 = 1100 \text{ nm}$.

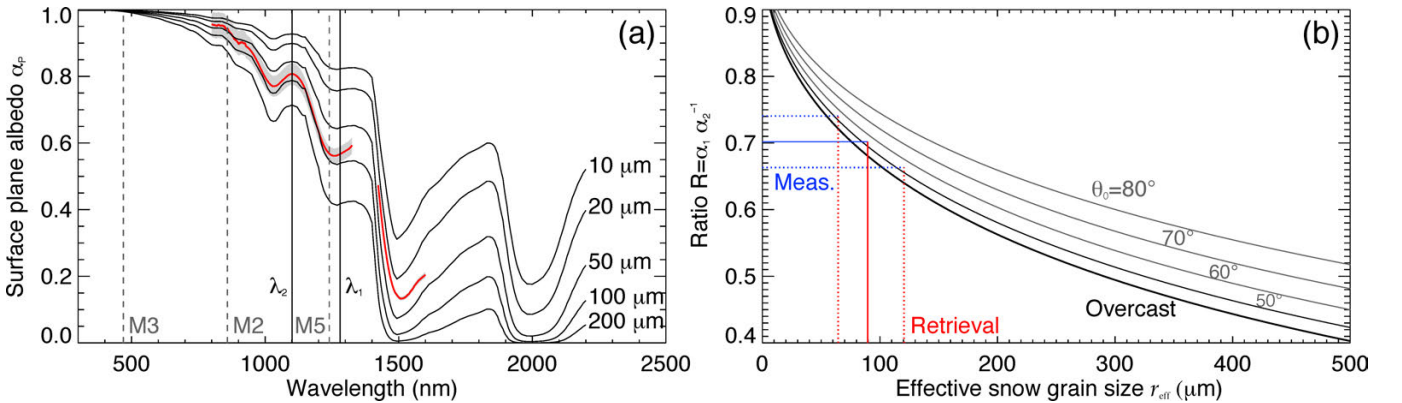


Figure 4. Left (a): Surface plane albedo for effective snow grain sizes between 10 μm and 200 μm , $\theta_0 = 60^\circ$, $A = 5.8$, χ -data from Warren and Brandt (2008). M3, M2, and M5 mark MODIS spectral bands used within the SGSP algorithm. λ_1 and λ_2 denote wavelengths used within the CORAS and SMART grain size retrieval. The red solid line and shaded gray show a spectral albedo measured by CORAS on 24 December 2013 (14 UTC). Right (b): Illustration of retrieval principle. Dependence of ratio \mathcal{R} with respect to effective snow grain size for different solar zenith angles (50° to 80°) and for overcast conditions, $A = 5.8$, χ -data from Warren and Brandt (2008). Blue and red lines illustrate the retrieval of effective snow grain size from a measured albedo ratio $\mathcal{R} = 0.7$ with a relative uncertainty of 35.5 %.

Figure 4a shows simulated snow surface plane albedos based on Eq. 10 Eqs. 3 and 8 for the wavelength range between 300 nm and 2200 nm for different effective snow grain sizes (10 μm to 200 μm) at 60° solar zenith angle ($A = 5.8$, χ -data from Warren and Brandt, 2008). In addition, it shows the MODIS channels used within the SGSP algorithm (M3, M2, and M5) and the spectral albedos α_p at wavelengths λ_1 and λ_2 used for calculating the albedo ratio \mathcal{R} . The spectra of α_p are related to the wavelength-dependence of the imaginary part of the complex refractive index of ice. Band M5 and

λ_1 are situated within a spectral albedo region which is more sensitive to effective snow grain size due to stronger absorption by ice. ~~The~~ Furthermore, a spectral albedo between 700 nm to 1600 nm wavelength measured by CORAS on 24 December 2013 (14 UTC) is shown. The data gap between 1300 nm and 1400 nm wavelength is due to low signal-to-noise ratios at these wavelengths. The retrieval principle is illustrated in Fig. 4b. For four different solar zenith angles ($\theta_0 = 50^\circ - 80^\circ$), it shows the dependence of the measured albedo ratio \mathcal{R} with respect to the effective snow grain size utilizing Eq. 12 ($A = 5.8$, χ -data from Warren and Brandt, 2008). Photons entering the snowpack under grazing angles have a higher probability of escaping the snowpack due to the pronounced forward scattering of ice crystals. This increases the spectral albedo mostly in the spectral range of stronger ice absorption. Therefore, \mathcal{R} increases with lower sun position. The overcast line in Fig. 4b corresponds to a solar zenith angle of around 50° under-in cloudless conditions, which is in accordance with Wiscombe and Warren (1980). The measurement uncertainty using of albedo measurements at 1280 nm wavelength was estimated with 6.8 %. Using \mathcal{R} , the uncertainty is reduced to 35.5 % as the transition to relative measurements yields independence from the radiometric calibration. Using independence from the cross-calibration. In addition to the instrumental errors, the surface slope at the footprint scale may influence the retrieval results. Using data from Picard et al. (2016), Dumont et al. (2017) found variations of the surface slope caused by wind drift at Dome C of $\pm 2^\circ$. They estimated a resulting uncertainty of 10 % in retrieved SSA due to these variations of the surface slope. Assuming a similar variability of the slope of the surface at Kohnen, an additional uncertainty of 10 % is assumed for the retrieval of SSA. Applying Eq. 12 ,to the spectral albedo measured by CORAS on 24 December 2013 (Fig. 4a), the measured ratio \mathcal{R} of 0.700 ± 0.021 would lead 0.039 leads to an estimated effective snow grain size of about $100 \pm 17 \mu\text{m}$ at $\theta_0 = 60^\circ$ (blue and red lines in Fig. 4b). However, the relative uncertainty of the retrieval varies with solar position and effective snow grain size. In general, it is higher for smaller snow grains. The Overall, the retrieval uncertainty ranges between 13 % and 37 % for the SSA throughout the measurement period.

3.2.1 Application in cloudless conditions

The retrieval algorithm was tested for specific measurements collected on a day with prevailing cloudless conditions. During this day, changes in effective snow grain size are expected to be small as the last snowfall took place six days earlier. Figure 5 shows the results retrieved from ground-based measurements with CORAS (SSA and effective snow grain size) on 24 December 2013 between 6 UTC and 18 UTC. Effective During this time, the solar zenith angle varied between 52° and 67° . Effective snow grain sizes were calculated according to Eq. 12 using the escape function $K_0(\theta_0)$ given by Eq. 3-4 (black line). The retrieved SSA shows a pronounced diurnal cycle and varies between $27.37 \pm 28.38 \text{ m}^2 \text{ kg}^{-1}$ ($r_{\text{eff}} = 90 - 120 \mu\text{m}$ $r_{\text{eff}} = 86 - 117 \mu\text{m}$). As no snowfall occurred on that day, the diurnal cycle is likely to be very likely an artefact originating from the change in solar zenith angle and the assumed escape function $K_0(\theta_0)$. The escape function approximation for the escape function (Eq. 4) might be incorrect if the snow BRDF is more complex due to the for snow at oblique incidence due to its elongated phase function. At the same time, a representative form factor A is required to account for the non-spherical snow grain shape. In order to

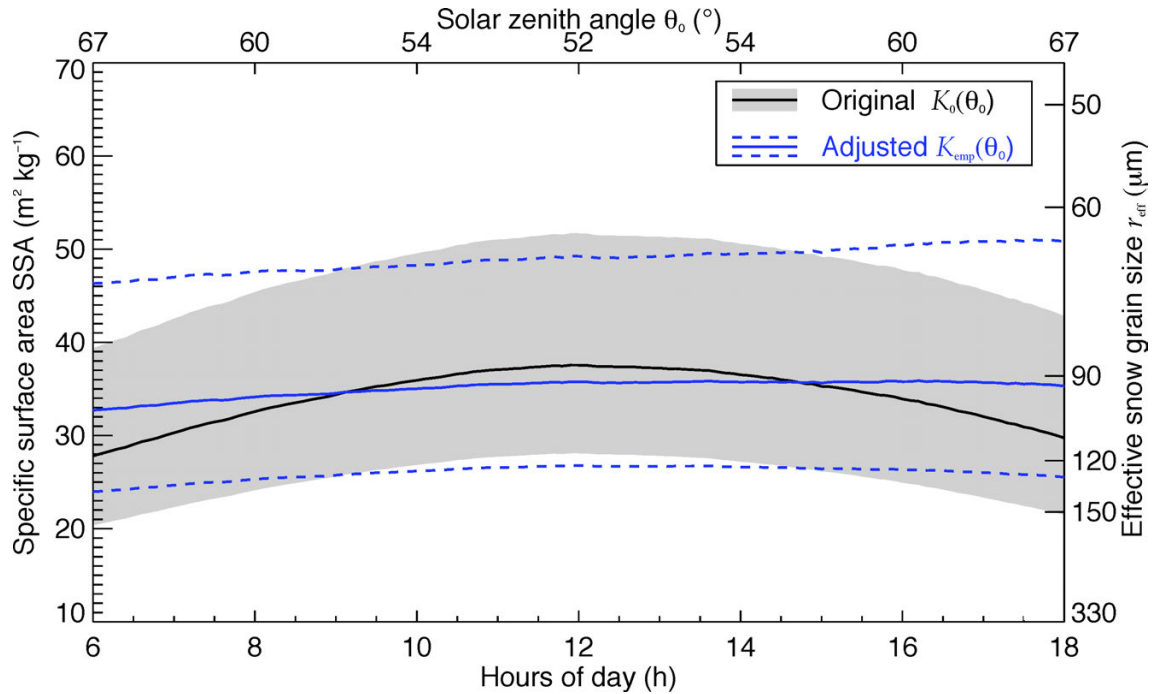


Figure 5. Diurnal cycle of SSA retrieved from CORAS measurements and effective snow grain size at Kohnen station on 24 December 2013. Black: SSA retrieved with original escape function $K_0(\theta_0)$ (solid line) with retrieval uncertainty (shaded gray), Blue: SSA retrieved with empirically adjusted escape function $K_{\text{emp}}(\theta_0)$ (solid line) and retrieval uncertainty (dashed lines).

eliminate the unrealistic diurnal cycle in the retrieved time series, the escape function was empirically adjusted to:

$$K_{\text{emp}}(\theta_0) = \frac{3}{7} (1.5 + 1.1 \cos \theta_0). \quad (13)$$

Applying K_{emp} , the diurnal cycle in the retrieved SSA was significantly reduced (blue line in Fig. 5). The SSA ranges only between ~~32-35~~33-36 $\text{m}^2 \text{kg}^{-1}$ (~~93-101~~91-99 μm). ~~Analyses of time series on~~ The analysis of measurements during other cloud-

5 less days showed similar features. Therefore, K_{emp} was applied for the entire period of measurements. However, it should be noted that the escape function K_{emp} from Eq. 13 is an empirical approximation for the cases investigated here. To derive a more general description of the escape function, more cases and explicit BRDF measurements are needed, which is beyond the scope of this study. Furthermore, Gallet et al. (2014b) observed SSA variations on a sub-daily scale using the DUFIS instrument (DUal Frequency Integrating Sphere for Snow SSA measurements; Gallet et al., 2009) at Dome C in January 2009.

10 They measured a drop in SSA at around noon from $40 \text{ m}^2 \text{kg}^{-1}$ to $33 \text{ m}^2 \text{kg}^{-1}$ before the SSA increased again to $41 \text{ m}^2 \text{kg}^{-1}$ at midnight. These temporal changes were attributed to the growth of sublimation crystals during daytime and nighttime formation of surface hoar. The SSA variations observed by CORAS on 24 December 2013 are in the same order of magnitude. However, the variations observed by Gallet et al. (2014b) are not symmetric to noon and their sign changes on a day-to-day scale due to the strong dependence on meteorological conditions. Even though an influence of crystal growth processes cannot be ruled out

for the measurements presented here, the evident dependence on the solar zenith angle and the constant symmetry to noon of the diurnal cycle observed in the SSA retrieved from CORAS measurements strongly indicate a dominating influence of the solar zenith angle.

To minimize the impact of solar zenith angle even further, measurements between 13 UTC and 14 UTC were preferably analyzed to represent the typical daily value of SSA and r_{eff} . Using these times of day additionally ensures higher upward and downward irradiances and, therefore, a reduced measurement uncertainty by enhanced signal-to-noise ratios. The retrieval time period is also close to the probing of in situ SSA between 15 and 18 UTC which is favorable for the comparison. For each day, the times when SSA was retrieved from measurements with CORAS are added to Fig. 1 as black open circles. It has to be noted that the cloud cover was estimated from visual observation every full hour, whereas CORAS measurements were partly analyzed for times in between the visual observation and the cloud cover given here might not be representative for the actual CORAS measurement (e.g., 5 octa on 27 December 2013). Therefore, the CORAS measurements were carefully screened for any cloud contamination by analyzing the downward solar irradiance to guarantee homogeneous cloudless or overcast conditions.

3.2.2 Extension to overcast conditions

The retrieval in overcast conditions was only applied when no cloudless period occurred during the day. ~~The original~~ Even though new approaches to retrieve effective snow grain size below liquid clouds from airborne remote sensing are available and potentially transferable to spaceborne observations (Ehrlich et al., 2017), the SGSP algorithm is restricted to cloud-free scenes. However, in case of ground-based measurements, the analysis can be extended to cloudy conditions by using the spherical albedo and assuming isotropic illumination by the clouds. In this case, the spherical albedo α_s can be expressed by using $K_0(\theta_0) = 1$ (isotropic) in Eq. 3 (Kokhanovsky and Zege, 2004):

$$\alpha_s = \exp(-y). \quad (14)$$

Using the albedo ratio \mathcal{R} in Eq. 12, the retrieved effective snow grain size is obtained in overcast conditions:

$$r_{\text{eff}}^{\text{cld}} = \left\{ \frac{\ln \mathcal{R}}{A \cdot \left[\sqrt{\frac{4\pi \chi(\lambda_2)}{\lambda_2}} - \sqrt{\frac{4\pi \chi(\lambda_1)}{\lambda_1}} \right]} \right\}^2. \quad (15)$$

Equation 15 is illustrated within Fig. 4b for comparison (overcast line). Retrievals in overcast conditions were applied on four days and are denoted as black filled circles in Fig. 1.

3.2.3 Retrieval using airborne measurements

For the airborne observations, SSA and r_{eff} were retrieved in a similar way as described above for ground-based data but using measurements of SMART. For comparison with the ground-based observations, any flight leg over the 5 x 5 pixel of MODIS surrounding Kohnen station (5 x 5 km²) is regarded as an overflight. The retrieval was not applied to each single measurement

point but to the mean albedo measured within this box. The uncertainties of the retrieval were estimated similarly to the ground-based CORAS measurements, with the exception that the uncertainty of irradiance measurements is assumed to be slightly higher due to the remaining uncertainty in the horizontal leveling of the airborne sensors by the horizontal stabilization of SMART (6.9 % at 1280 nm wavelength). As a result, the estimated uncertainty of the measured albedo ratio \mathcal{R} is about 3.35,6 %.

3.3 Influence of wavelength choice

The in situ measurements and all retrievals (in the original and adapted SGSP algorithm) use different wavelengths. Therefore, each instrument retrieves the effective snow grain size from a different depth within the snowpack. All retrievals considered in this study were performed neglecting snow layer stratification. Vertical differences in snow grain size can impose systematic differences in the retrieved values between the various instruments. To quantify the impact of the choice of wavelength, the e-folding depth $\epsilon(\lambda)$ was calculated. It, which is defined as the distance in the snowpack over which the irradiance reduces to $1/e$ or 37 % of the incident value and is wavelength-dependent. Following Zege et al. (1991), it is calculated by:

$$\epsilon(\lambda) = \left\{ 3 \frac{\rho_{\text{snow}}}{\rho_{\text{ice}}} \cdot \sqrt{2\pi \cdot \frac{\chi}{\lambda r_{\text{eff}}} \cdot B(\xi) \cdot [1 - g(\xi)]} \right\}^{-1}. \quad (16)$$

The calculation assumed a mixture of hexagonal plates and columns ($A = 5.8$). The IceCube system penetrates 0.14-0.31 cm into the snowpack at 1310 nm (at snow densities between 280 and 360 kg m⁻³). At the wavelengths more sensitive to ice absorption, CORAS (SMART) mainly measures photons reflected in a depth up to 0.30 cm (at 1280 nm) and MODIS channel 5 (1240 nm) receives reflected radiation from a depth similar to the IceCube system. Hence, the penetration depth is almost identical for all measurement devices reducing its potential influence on the differences in the retrieved SSA signal which allows a comparison of the different SSA retrievals.

4 Results and discussion

Figure 6 shows the time series of SSA and respective effective snow grain size derived from satellite (MODIS, red), ground-based (CORAS, blue) and airborne (SMART, green) observations between 10 December 2013 and 31 January 2014 at Kohnen station. For comparison, the in situ data from Freitag et al. (in prep.) are shown in black.

4.1 SSA and effective snow grain size from CORAS (ground-based)

SSA retrieved from CORAS measurements (blue circles in Fig. 6) varied between 27 m² kg⁻¹ and 86,89 m² kg⁻¹ throughout the campaign. The evolution of the time series revealed four pronounced maxima (minima in r_{eff}) on 18 December 2013, 3, 17, and 22 January 2014, which can be related to snowfall of about 1 mm at Kohnen (visual estimation). The fresh fallen snow consists of smaller grains which increases SSA of the uppermost snow layer. The average snowfall-induced increase in SSA is 28 m² kg⁻¹. These highest SSA values are followed by a gradual decrease in SSA. From 18 to 30 December 2013, the SSA decreased daily by approximately 3.2 m² kg⁻¹ d⁻¹ from 65,66 m² kg⁻¹ to 27 m² kg⁻¹. This corresponds to an increase

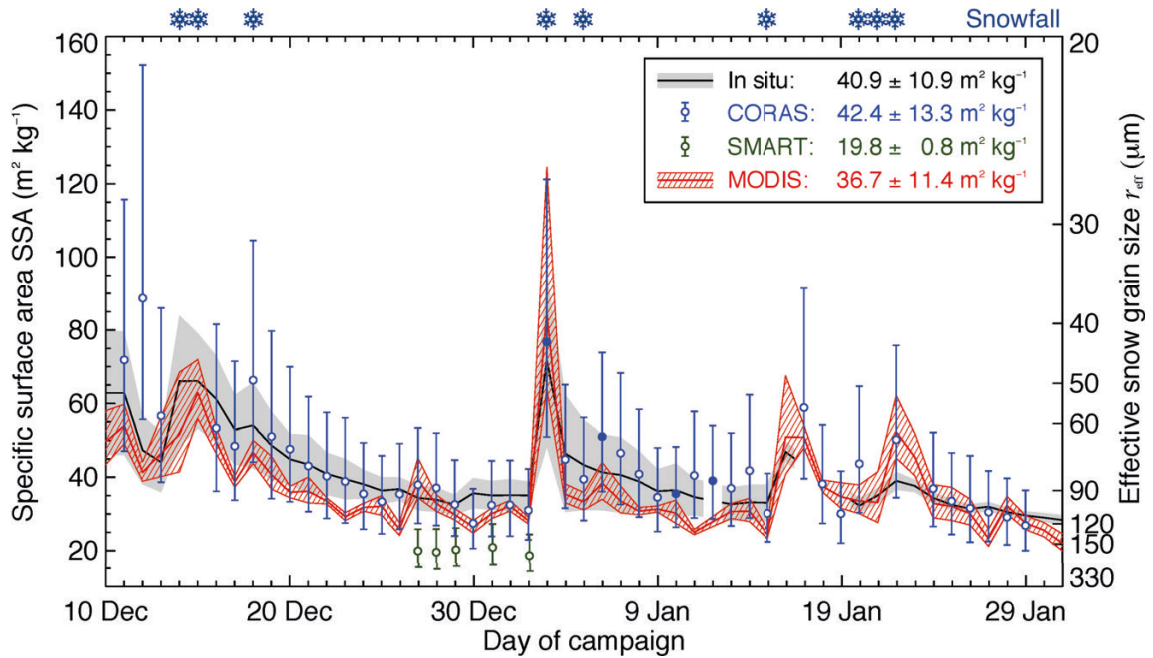


Figure 6. Time series of measured SSA and r_{eff} for the entire campaign at Kohnen station. Black: Mean (solid line) and standard deviation (shaded gray) for in situ measurements (data from: Freitag et al., in prep.). Red: MODIS retrieval, Blue: CORAS retrieval in cloudless (open circles) and overcast (filled circles) conditions, Green: SMART retrieval in cloudless (open circles) conditions. Top right: mean and standard deviation of the SSA retrieved by the different instruments. Snowflake symbols denote snowfall events.

in effective snow grain size by $5.9 \pm 5.8 \mu\text{m}$ per day. This decrease in SSA is slightly slower than measured by Libois et al. (2015) at Dome C ($75^\circ 6' \text{ S}, 123^\circ 0' \text{ E}$), Antarctica. They observed a drop in SSA from $90 \text{ m}^2 \text{ kg}^{-1}$ to $30 \text{ m}^2 \text{ kg}^{-1}$ within 10 days due to snow metamorphism. However, some abrupt decreases in SSA such as from 3 to 4 January 2014 cannot be explained by metamorphism alone, especially under the cold conditions on the Antarctic plateau. Instead, this strong increase in effective

5 snow grain size within one day is supposedly caused by strong wind, which removes the small, fresh fallen snow grains and exposes deeper layers of larger grains. With mean wind speeds of 4 m s^{-1} and maximum wind gusts reaching 11 m s^{-1} at Kohnen station, drifting snow occurred mainly due to creeping or saltation of the ice crystals. This wind-induced transportation of fresh fallen snow grains is superimposed on the signal of snow metamorphism in the temporal evolution of SSA retrieved from CORAS.

10 The mean SSA is $42 \pm 13 \text{ m}^2 \text{ kg}^{-1}$. The SSA retrieved from CORAS measurements reproduces the in situ probing (solid black line in Fig. 6) within the measurement uncertainties and range within the shaded gray area, which indicates the standard deviation of the mean SSA value along the 100 m-transect where SSA was probed. The standard deviation is a measure of the small-scale variability in SSA mainly caused by wind-induced roughness structures of the snow surface. Nevertheless, the temporal signal in SSA is significant for all sample positions. Only during the end of the campaign, the last two snowfall-

induced maxima in SSA are overestimated by CORAS. The agreement between the SSA retrieved by CORAS and the in situ data is reflected in the linear correlation coefficient of 0.81 (95 % confidence interval: ~~0.67~~0.66-0.89).

On eight days throughout the campaign, no retrieval of SSA using CORAS data was possible due to broken clouds. For that reason, ~~e.g.~~, the first maximum of the in situ measured SSA (15 December 2013) could not be reproduced by CORAS data. Overcast retrieval conditions were used on four days (filled circles: 3, 6, 10, and 12 January 2014). The retrieved SSA on overcast days agree well with the in situ measurements and are in coherence with the retrieved SSA under cloudless conditions. This illustrates the potential of extending the retrieval method by applying the spherical albedo. In addition, it highlights the benefit of ground-based observations that, in comparison to satellite observations, provide continuous time series and are not restricted to cloudless time periods only.

10 4.2 SSA and effective snow grain size from SMART (airborne)

On five days between 27 December 2013 and 2 January 2014, SSA and r_{eff} were retrieved from airborne spectral albedo measurements by SMART (green circles in Fig. 6). With a mean value of $20 \pm 1 \text{ m}^2 \text{ kg}^{-1}$, SMART seems to systematically underestimate in situ SSA by a factor of 2.1. Using the same calibration reference and the identical retrieval algorithm for both CORAS and SMART, the differences are likely connected to the different sizes of the sampling areas covered by both instruments. While CORAS measurements represent a spot of about $2 \times 2 \text{ m}^2$, SMART measurements have a larger footprint and were averaged over an area of $5 \times 5 \text{ km}^2$ surrounding Kohnen station. Furthermore, the area over which the airborne data is averaged is largely determined by the flight track. On such scales, the local small-scale variability of SSA as indicated by the in situ measurements can lead to significant differences in SSA. Already along the 100 m-transect, in situ SSA varied by up to 34 % (4 January 2014). On larger scales, this variability is likely to increase. In addition, unidentified systematical errors in the airborne SMART measurements are a possible reason for the underestimation of SSA and deserve further attention in future studies.

20 4.3 SSA and effective snow grain size from MODIS (spaceborne)

A smaller bias is present in the SSA retrieved from MODIS data ($37 \pm 11 \text{ m}^2 \text{ kg}^{-1}$, red line in Fig. 6), which integrates over an area of $50 \times 50 \text{ km}^2$ surrounding Kohnen station. The uncertainty in Fig. 6 is given as the standard deviation of SSA over the $50 \times 50 \text{ km}^2$. The SSA derived from MODIS observations could reproduce the SSA signal from in situ measurements, the linear correlation coefficient is with 0.86 (95% confidence interval: 0.75-0.92) slightly higher than for the CORAS measurements. Furthermore, it was able to resolve abrupt changes in SSA due to precipitation or wind-induced transportation of snow grains. For high solar zenith angles, the SGSP algorithm is known to underestimate the actual effective snow grain size (Zege et al., 2011). During the entire observation period, the solar zenith angle varied between 52° and 87° and in 48 % of the time was higher than 70° . However, the effective snow grain size retrieved from MODIS data mostly showed a slight overestimation compared to the in situ measurements. The comparison of the ground-based (CORAS) and spaceborne (MODIS) remote sensing methods to retrieve SSA yields a linear correlation coefficient of 0.77 (95 % confidence interval: 0.61-0.87) which lies in the same range as the correlation coefficient between CORAS and the in situ measurements.

5 Conclusions

The temporal variability of SSA and respective r_{eff} on the East Antarctic plateau were investigated during austral summer 2013/14 utilizing spectral albedo measurements (ground-based and airborne) and MODIS reflectance measurements. The retrieved SSA and r_{eff} were compared with in situ data.

- 5 For the retrievals from spectral surface albedo measurements, the SGSP algorithm was extended to spectral ratios of albedo at 1280 nm and 1100 nm wavelength. Being independent of systematic measurement uncertainties (e.g., ~~radiometric calibration~~cross-calibration of the optical inlets), this approach decreases the uncertainty of the retrieved SSA compared to the single-wavelength approach. The retrieval was successfully applied to measurements in overcast conditions by using the spherical instead of the plane albedo. Satellite observations are limited by clouds in space and time. During the two months
10 of observations at Kohnen station, cloudless conditions were present only 264 h out of 1272 h total observation time (21 %). However, many cloudy periods were characterized by a broken cloud field (62 % of total observation time). In this case, the concept of spherical albedo is not applicable and SSA retrievals might fail. Therefore, only overcast conditions were included in the analysis.

- SSA retrieved from CORAS measurements varied between $27 \text{ m}^2 \text{ kg}^{-1}$ and ~~86~~89 $\text{m}^2 \text{ kg}^{-1}$ and revealed distinct maxima
15 related to light snowfall at Kohnen station. The average increase in SSA due to snowfall was $28 \text{ m}^2 \text{ kg}^{-1}$. The maxima were followed by a gradual decrease in SSA, which was partly caused by snow metamorphism and by wind-induced transport of the fresh fallen ice crystals. During the longest dry period (18 until 30 December 2013), SSA decreased on average by $3.2 \text{ m}^2 \text{ kg}^{-1}$ per day. This corresponded to a daily increase of r_{eff} by ~~5.9~~5.8 μm .

- The temporal evolution of SSA retrieved from the ground-based CORAS measurements could reproduce the in situ mea-
20 surements (linear correlation coefficient: 0.81). The same holds true for the spaceborne MODIS retrieval (0.86). Despite the biases in SSA retrieved from the different instruments, the agreement especially between SSA retrieved from CORAS and in situ measurements emphasizes the potential of the retrieval algorithms. SSA retrieved from airborne SMART measurements underestimated in situ SSA by a factor of 2.1. This might be due to spatial averaging. However, especially the differences between SSA derived from CORAS and SMART measurements need to be investigated in more detail in further research,
25 before extending the retrieval validation between SMART and MODIS to a larger area in Dronning Maud Land which would also cover coastal areas with supposedly higher variability in SSA. An Antarctic-wide survey of albedo mapping can only be achieved by satellite observations. For this purpose, a more detailed understanding of the relation between satellite and in situ observation of SSA is required, including the influence of the different spatial scales of satellite, airborne, and in situ measurements.

- 30 The validation presented in this study provided an unique testbed for retrievals of effective snow grain size from satellite reflectance and spectral surface albedo measurements under Antarctic conditions where in situ data are scarce and can be used for testing prognostic snowpack models in Antarctic conditions.

Acknowledgements. This work was supported by the Deutsche Forschungsgemeinschaft (DFG) in the framework of the priority programme “Antarctic Research with comparative investigations in Arctic ice areas” (SPP 1158) by the grants WE1900/29-1 and BI 816/4-1. We gratefully acknowledge the support by the SFB/TR 172 “Arctic Amplification: Climate Relevant Atmospheric and Surface Processes, and Feedback Mechanisms (AC)”³ funded by the DFG. We are grateful to the Alfred Wegener Institute, Helmholtz Centre for Polar and Marine Research, Bremerhaven, Germany for supporting the campaign with logistics, the aircraft and manpower in Antarctica. In addition, we would like to thank Kenn Borek Air Ltd., Calgary, Canada for the great pilots who made the complicated measurements possible.

5

References

- Birnbaum, G., Brauner, R., and Ries, H.: Synoptic situations causing high precipitation rates on the Antarctic plateau: observations from Kohnen Station, Dronning Maud Land, *Antarct. Sci.*, 18, 279–288, doi:10.1017/S0954102006000320, 2006.
- Bohren, C. and Barkstrom, B.: Theory of the optical properties of snow, *J. Geophys. Res.*, 79, 4527–4535, 1974.
- 5 Bond, T. C., Doherty, S. J., Fahey, D. W., Forster, P. M., Berntsen, T., DeAngelo, B. J., Flanner, M. G., Ghan, S., Karcher, B., Koch, D., Kinne, S., Kondo, Y., Quinn, P. K., Sarofim, M. C., Schultz, M. G., Schulz, M., Venkataraman, C., Zhang, H., Zhang, S., Bellouin, N., Guttikunda, S. K., Hopke, P. K., Jacobson, M. Z., Kaiser, J. W., Klimont, Z., Lohmann, U., Schwarz, J. P., Shindell, D., Storelvmo, T., Warren, S. G., and Zender, C. S.: Bounding the role of black carbon in the climate system: A scientific assessment, *J. Geophys. Res.*, 118, 5380–5552, doi:10.1002/jgrd.50171, 2013.
- 10 Brückner, M., Pospichal, B., Macke, A., and Wendisch, M.: A new multispectral cloud retrieval method for ship-based solar transmissivity measurements, *J. Geophys. Res.*, 119, 11.338–11.354, doi:10.1002/2014JD021775, 2014.
- Burton-Johnson, A., Black, M., Fretwell, P. T., and Kaluza-Gilbert, J.: An automated methodology for differentiating rock from snow, clouds and sea in Antarctica from Landsat 8 imagery: a new rock outcrop map and area estimation for the entire Antarctic continent, *The Cryosphere*, 10, 1665–1677, 2016.
- 15 Colbeck, S. C.: Theory of Metamorphism of Dry Snow, *J. Geophys. Res.*, 88, 5475–5482, doi:10.1029/JC088iC09p05475, 1983.
- Dang, C., Brandt, R. E., and Warren, S. G.: Parameterizations for narrowband and broadband albedo of pure snow and snow containing mineral dust and black carbon, *J. Geophys. Res.*, 120, 5446–5468, doi:10.1002/2014JD022646, 2015.
- Dang, C., Fu, Q., and Warren, S. G.: Effect of Snow Grain Shape on Snow Albedo, *J. Atmos. Sci.*, 73, 3573–3583, doi:10.1175/JAS-D-15-0276.1, 2016.
- 20 Domine, F., Cabanes, A., Taillandier, A. S., and Legagneux, L.: Specific surface area of snow samples determined by CH₄ adsorption at 77 K and estimated by optical microscopy and scanning electron microscopy, *Environ. Sci. Technol.*, 35, 771–780, doi:10.1021/es001168n, 2001.
- Domine, F., Salvatori, R., Legagneux, L., Salzano, R., Fily, M., and Casacchia, R.: Correlation between the specific surface area and the short wave infrared (SWIR) reflectance of snow, *Cold Reg. Sci. Technol.*, 46, 60–68, doi:10.1016/j.coldregions.2006.06.002, 2006.
- 25 Dumont, M., Brissaud, O., Picard, G., Schmitt, B., Gallet, J. C., and Arnaud, Y.: High-accuracy measurements of snow Bidirectional Reflectance Distribution Function at visible and NIR wavelengths - comparison with modelling results, *Atmos. Chem. Phys.*, 10, 2507–2520, doi:10.5194/acp-10-2507-2010, 2010.
- Dumont, M., Arnaud, L., Picard, G., Libois, Q., Lejeune, Y., Nabat, P., Voisin, D., and Morin, S.: In situ continuous visible and near-infrared spectroscopy of an alpine snowpack, *The Cryosphere*, 11, 1091–1110, doi:10.5194/tc-11-1091-2017, 2017.
- 30 Ehrlich, A., Bierwirth, E., Wendisch, M., Gayet, J.-F., Mioche, G., Lampert, A., and Heintzenberg, J.: Cloud phase identification of Arctic boundary-layer clouds from airborne spectral reflection measurements: Test of three approaches, *Atmos. Chem. Phys.*, 8, 7493–7505, doi:10.5194/acp-8-7493-2008, 2008.
- Ehrlich, A., Bierwirth, E., Wendisch, M., Herber, A., and Gayet, J. F.: Airborne hyperspectral observations of surface and cloud directional reflectivity using a commercial digital camera, *Atmos. Chem. Phys.*, 12, 3493–3510, doi:10.5194/acp-12-3493-2012, 2012.
- 35 Ehrlich, A., Bierwirth, E., Istomina, L., and Wendisch, M.: Combined retrieval of Arctic liquid water cloud and surface snow properties using airborne spectral solar remote sensing, *Atmos. Meas. Tech. Discuss.*, doi:10.5194/amt-2017-50, in review, 2017.

- Fierz, C., Armstrong, R. L., Durand, Y., Etchevers, P., Greene, E., McClung, D. M., Nishimura, K., Satyawali, P. K., and Sokratov, S. A.: The International Classification for Seasonal Snow on the Ground, IHP-VII Technical Documents in Hydrology N°83, IACS Contribution N°1, UNESCO-IHP, Paris, 2009.
- Flin, F., Brzoska, J. B., Coeurjolly, D., Pieritz, R. A., Lesaffre, B., Coleou, C., Lambole, P., Teytaud, O., Vignoles, G. L., and Delesse, J. F.: Adaptive estimation of normals and surface area for discrete 3-D objects: Application to snow binary data from X-ray tomography, *IEEE Trans. Image Process.*, 14, 585–596, doi:10.1109/TIP.2005.846021, 2005.
- Freitag, J., Klein, K., Kipfstuhl, S., Birnbaum, G., Schneebeli, M., and Orsi, A.: Seasonal development of specific surface area of snow in East Antarctica: Observations from Kohnen-Station, Dronning Maud Land., *Geophys. Res. Lett.*, in prep.
- Gallet, J. C., Domine, F., Zender, C. S., and Picard, G.: Measurement of the specific surface area of snow using infrared reflectance in an integrating sphere at 1310 and 1550 nm, *The Cryosphere*, 3, 167–182, 2009.
- Gallet, J. C., Domine, F., and Dumont, M.: Measuring the specific surface area of wet snow using 1310 nm reflectance, *The Cryosphere*, 8, 1139–1148, doi:10.5194/tc-8-1139-2014, 2014a.
- Gallet, J. C., Domine, F., Savarino, J., Dumont, M., and Brun, E.: The growth of sublimation crystals and surface hoar on the Antarctic plateau, *The Cryosphere*, 8, 1205–1215, doi:10.5194/tc-8-1205-2014, 2014b.
- Grenfell, T. C. and Warren, S. G.: Representation of a nonspherical ice particle by a collection of independent spheres for scattering and absorption of radiation, *J. Geophys. Res.*, 104, 31.697–31.709, doi:10.1029/1999JD900496, 1999.
- Grenfell, T. C., Warren, S. G., and Mullen, P. C.: Reflection of solar radiation by the Antarctic snow surface at ultraviolet, visible, and near-Infrared wavelengths, *J. Geophys. Res.*, 99, 18.669–18.684, doi:10.1029/94JD01484, 1994.
- Hansen, J. and Nazarenko, L.: Soot climate forcing via snow and ice albedos, *Proc. Natl. Acad. Sci. U. S. A.*, 101, 423–428, doi:10.1073/pnas.2237157100, 2004.
- Hudson, S. R., Warren, S. G., Brandt, R. E., Grenfell, T. C., and Six, D.: Spectral bidirectional reflectance of Antarctic snow: Measurements and parameterization, *J. Geophys. Res.*, 111, D18 106, doi:10.1029/2006JD007290, 2006.
- Jin, Z., Charlock, T. P., Yang, P., Xie, Y., and Miller, W.: Snow optical properties for different particle shapes with application to snow grain size retrieval and MODIS/CERES radiance comparison over Antarctica, *Rem. Sens. Env.*, 112, 3563–3581, doi:10.1016/j.rse.2008.04.011, 2008.
- Kaempfer, T. U. and Schneebeli, M.: Observation of isothermal metamorphism of new snow and interpretation as a sintering process, *J. Geophys. Res.*, 112, D24 101, doi:10.1029/2007JD009047, 2007.
- Kneizys, F. X., Abreu, L. W., Anderson, G. P., Chetwynd, J. H., Shettle, E. P., Berk, A., Bernstein, L. S., Robertson, D. C., Acharya, P. K., Rothman, L. A., Selby, J. E. A., Gallery, W. O., and Clough, S. A.: The MODTRAN 2/3 Report and LOWTRAN 7 MODEL., Phillips Laboratory Hanscom AFB, Bedford, 1996.
- Kokhanovsky, A. and Macke, A.: Integral light-scattering and absorption characteristics of large, nonspherical particles, *Appl. Opt.*, 36, 8785–8790, doi:10.1364/AO.36.008785, 1997.
- Kokhanovsky, A. A. and Zege, E. P.: Scattering optics of snow, *Appl. Opt.*, 43, 1589–1602, doi:10.1364/AO.43.001589, 2004.
- Legagneux, L., Cabanes, A., and Domine, F.: Measurement of the specific surface area of 176 snow samples using methane adsorption at 77 K, *J. Geophys. Res.*, 107, 4335, doi:10.1029/2001JD001016, 2002.
- Leppänen, L., Kontu, A., Vehviläinen, J., Lemmetyinen, J., and Pulliainen, J.: Comparison of traditional and optical grain-size field measurements with SNOWPACK simulations in a taiga snowpack, *J. Glaciol.*, 61, 151–162, doi:10.3189/2015JoG14J026, 2015.

- Libois, Q., Picard, G., France, J. L., Arnaud, L., Dumont, M., Carmagnola, C. M., and King, M. D.: Influence of grain shape on light penetration in snow, *The Cryosphere*, 7, 1803–1818, doi:10.5194/tc-7-1803-2013, 2013.
- Libois, Q., Picard, G., Dumont, M., Arnaud, L., Sergeant, C., Pougatch, E., Sudul, M., and Vial, D.: Experimental determination of the absorption enhancement parameter of snow, *J. Glaciol.*, 60, 714–724, doi:10.3189/2014JoG14J015, 2014.
- 5 Libois, Q., Picard, G., Arnaud, L., Dumont, M., Lafaysse, M., Morin, S., and Lefebvre, E.: Summertime evolution of snow specific surface area close to the surface on the Antarctic Plateau, *The Cryosphere*, 9, 2383–2398, doi:10.5194/tc-9-2383-2015, 2015.
- Lyapustin, A., Tedesco, M., Wang, Y., Aoki, T., Hori, M., and Kokhanovsky, A.: Retrieval of snow grain size over Greenland from MODIS, *Remote Sens. Environ.*, 113, 1976–1987, doi:10.1016/j.rse.2009.05.008, 2009.
- Matzl, M. and Schneebeli, M.: Stereological measurement of the specific surface area of seasonal snow types: Comparison to other methods, and implications for mm-scale vertical profiling, *Cold Reg. Sci. Technol.*, 64, 1–8, doi:10.1016/j.coldregions.2010.06.006, 2010.
- 10 Mayer, B. and Kylling, A.: Technical note: The *libRadtran* software package for radiative transfer calculations - description and examples of use, *Atmos. Chem. Phys.*, 5, 1855–1877, doi:10.5194/acp-5-1855-2005, 2005.
- Munneke, P. K., Reijmer, C. H., van den Broeke, M. R., König-Langlo, G., Stammes, P., and Knap, W. H.: Analysis of clear-sky Antarctic snow albedo using observations and radiative transfer modeling RID G-8736-2011 RID F-7867-2011, *J. Geophys. Res.*, 113, D17 118, doi:10.1029/2007JD009653, 2008.
- 15 Myhre, G., Shindell, D., Bréon, F.-M., Collins, W., Fuglestad, J., Huang, J., Koch, D., Lamarque, J.-F., Lee, D., Mendoza, B., Nakajima, T., Robock, A., Stephens, G., Takemura, T., and Zhang, H.: Anthropogenic and Natural Radiative Forcing, in: *Climate Change 2013: The Physical Science Basis. Contribution of Working Group I to the Fifth Assessment Report of the Intergovernmental Panel on Climate Change*, edited by Stocker, T., Qin, D., Plattner, G.-K., Tignor, M., Allen, S., Boschung, J., Nauels, A., Xia, Y., Bex, V., and Midgley, P., Cambridge University Press, Cambridge, United Kingdom and New York, NY, USA, doi:10.1017/CBO9781107415324.018, 2013.
- 20 Neshyba, S. P., Grenfell, T. C., and Warren, S. G.: Representation of a nonspherical ice particle by a collection of independent spheres for scattering and absorption of radiation: 2. Hexagonal columns and plates, *J. Geophys. Res.*, 108, Art. No. 4448, doi:10.1029/2002JD003302, 2003.
- Oerter, H., Wilhelms, F., Jung-Rothenhauser, F., Goktas, F., Miller, H., Graf, W., and Sommer, S.: Accumulation rates in Dronning Maud Land, Antarctica, as revealed by dielectric-profiling measurements of shallow firn cores, *Ann. Glaciol.*, 30, 27–34, doi:10.3189/172756400781820705, 2000.
- 25 Picard, G., Libois, Q., Arnaud, L., Verin, G., and Dumont, M.: Development and calibration of an automatic spectral albedometer to estimate near-surface snow SSA time series, *The Cryosphere*, 10, 1297–1316, doi:10.5194/tc-10-1297-2016, 2016.
- Picard, G., Arnaud, L., Domine, F., and Fily, M.: Determining snow specific surface area from near-infrared reflectance measurements: Numerical study of the influence of grain shape, *Cold Reg. Sci. Technol.*, 56, 10–17, doi:10.1016/j.coldregions.2008.10.001, 2009.
- 30 Picard, G., Domine, F., Krinner, G., Arnaud, L., and Lefebvre, E.: Inhibition of the positive snow-albedo feedback by precipitation in interior Antarctica, *Nat. Clim. Chang.*, 2, 795–798, doi:10.1038/NCLIMATE1590, 2012.
- Schaepman-Strub, G., Schaepman, M. E., Painter, T. H., Dangel, S., and Martonchik, J. V.: Reflectance quantities in optical remote sensing-definitions and case studies, *Remote Sens. Environ.*, 103, 27–42, 2006.
- 35 Singh, P.: *Snow and Glacier Hydrology*, Water Science and Technology Library, Springer Netherlands, 2001.
- Stammes, K., Tsay, S., Wiscombe, W., and Jayaweera, K.: A numerically stable algorithm for discrete-ordinate-method radiative transfer in multiple scattering and emitting layered media, *Appl. Opt.*, 27, 2502–2509, doi:10.1364/AO.27.002502, 1988.

- Tomasi, C., Vitale, V., Lupi, A., Di Carmine, C., Campanelli, M., Herber, A., Treffeisen, R., Stone, R. S., Andrews, E., Sharma, S., Radionov, V., von Hoyningen-Huene, W., Stebel, K., Hansen, G. H., Myhre, C. L., Wehrli, C., Aaltonen, V., Lihavainen, H., Virkkula, A., Hillamo, R., Strom, J., Toledano, C., Cachorro, V. E., Ortiz, P., de Frutos, A. M., Blindheim, S., Frioud, M., Gausa, M., Zielinski, T., Petelski, T., and Yamanouchi, T.: Aerosols in polar regions: A historical overview based on optical depth and in situ observations, *J. Geophys. Res.*, 112, D16 205, doi:10.1029/2007JD008432, 2007.
- 5 Tynes, H., Kattawar, G., Zege, E., Katsev, I., Prikhach, A., and Chaikovskaya, L.: Monte Carlo and multicomponent approximation methods for vector radiative transfer by use of effective Mueller matrix calculations, *Appl. Opt.*, 40, 400–412, doi:10.1364/AO.40.000400, 2001.
- Vaughan, D., Comiso, J., Allison, I., Carrasco, J., Kaser, G., Kwok, R., Mote, P., Murray, T., Paul, F., Ren, J., Rignot, E., Solomina, O., Steffen, K., and Zhang, T.: Observations: Cryosphere, in: *Climate Change 2013: The Physical Science Basis. Contribution of Working Group I to the Fifth Assessment Report of the Intergovernmental Panel on Climate Change*, edited by Stocker, T., Qin, D., Plattner, G.-K., Tignor, M., Allen, S., Boschung, J., Nauels, A., Xia, Y., Bex, V., and Midgley, P., Cambridge University Press, Cambridge, United Kingdom and New York, NY, USA, doi:10.1017/CBO9781107415324.012, 2013.
- 10 Warren, S., Brandt, R., and O’Rawe Hinton, P.: Effect of surface roughness on bidirectional reflectance of Antarctic snow, *J. Geophys. Res.*, 103, 25 789–25 807, doi:10.1029/98JE01898, 1998.
- 15 Warren, S. G. and Brandt, R. E.: Optical constants of ice from the ultraviolet to the microwave: A revised compilation, *J. Geophys. Res.*, 113, Art. No. D14 220, doi:10.1029/2007JD009744, 2008.
- Wendisch, M., Müller, D., Schell, D., and Heintzenberg, J.: An airborne spectral albedometer with active horizontal stabilization, *J. Atmos. Oceanic Technol.*, 18, 1856–1866, doi:10.1175/1520-0426(2001)018<1856:AASAWA>2.0.CO;2, 2001.
- Wendisch, M., Pilewskie, P., Jäkel, E., Schmidt, S., Pommier, J., Howard, S., Jonsson, H. H., Guan, H., Schröder, M., and Mayer, B.: Airborne measurements of areal spectral surface albedo over different sea and land surfaces, *J. Geophys. Res.*, 109, Art. No. D08 203, doi:10.1029/2003JD004392, 2004.
- 20 Werner, F., Siebert, H., Pilewskie, P., Schmeissner, T., Shaw, R. A., and Wendisch, M.: New airborne retrieval approach for trade wind cumulus properties under overlying cirrus, *J. Geophys. Res.*, 118, 3634–3649, doi:10.1002/jgrd.50334, 2013.
- Wiebe, H., Heygster, G., Zege, E., Aoki, T., and Hori, M.: Snow grain size retrieval SGSP from optical satellite data: Validation with ground measurements and detection of snow fall events, *Remote Sens. Environ.*, 128, 11–20, doi:10.1016/j.rse.2012.09.007, 2013.
- 25 Wiscombe, W.: Improved Mie scattering algorithms, *Appl. Opt.*, 19, 1505–1509, doi:10.1364/AO.19.001505, 1980.
- Wiscombe, W. and Warren, S.: A model for the spectral albedo of snow I. Pure snow, *J. Atmos. Sci.*, 37, 2712–2733, doi:10.1175/1520-0469(1980)037<2712:AMFTSA>2.0.CO;2, 1980.
- Zege, E., Ivanov, A., and Katsev, I.: *Image Transfer Through a Scattering Medium*, Springer-Verlag, Heidelberg, 1991.
- 30 Zege, E. P., Katsev, I. L., Malinka, A. V., Prikhach, A. S., Heygster, G., and Wiebe, H.: Algorithm for retrieval of the effective snow grain size and pollution amount from satellite measurements, *Remote Sens. Environ.*, 115, 2674–2685, doi:10.1016/j.rse.2011.06.001, 2011.

Table 1. List of instruments operated on ground and on Polar 6 aircraft.

	Instrument	Measured quantity	Specifications
Ground-based (Kohnen)	Kipp & Zonen CM22	F^\downarrow, F^\uparrow (W m^{-2})	Broadband, 0.2-3.6 μm
	Eppley Precision Infrared Radiometer	F^\downarrow, F^\uparrow (W m^{-2})	Broadband, 3.5-50 μm
	CORAS	$F^\downarrow(\lambda), F^\uparrow(\lambda)$ ($\text{W m}^{-2} \text{ nm}^{-1}$)	Spectral, 0.3-2.2 μm
	CANON EOS 6D	I^\uparrow ($\text{W m}^{-2} \text{ nm}^{-1} \text{ sr}^{-1}$)	180° fish-eye lens
	CANON EOS 600D	All-sky images	
	CANON EOS 600D (2x)	Photogrammetric images	Image overlap: 50 %
	Sun photometer SP1A31	AOD	10 channels: 368.5 to 1019.4 nm
	Automatic weather station	$p, T, \text{RH}, F^\uparrow, F^\downarrow, \vec{v}$, snow accumulation	1 min averages
	Ultrasonic anemometer	\vec{v}	
	Radio sounding	p, T, RH, \vec{v}	
	Synoptic observations	Cloud cover, precipitation	Visual observation
	IceCube by A2 Photonic Sensors	SSA ($\text{m}^2 \text{ kg}^{-1}$), ρ_{snow} (kg m^{-3})	Wavelength: 1310 nm
	Pt-100	Snow temperature profile	
Airborne (Polar 6)	Kipp & Zonen CMP22	F^\downarrow, F^\uparrow (W m^{-2})	Broadband, 0.2-3.6 μm
	Kipp & Zonen CGR4	F^\downarrow, F^\uparrow (W m^{-2})	Broadband, 4.5-42 μm
	SMART	$F^\downarrow(\lambda), F^\uparrow(\lambda)$ ($\text{W m}^{-2} \text{ nm}^{-1}$)	Spectral, 0.3-2.2 μm
		$I^\downarrow(\lambda), I^\uparrow(\lambda)$ ($\text{W m}^{-2} \text{ nm}^{-1} \text{ sr}^{-1}$)	Spectral, 0.3-2.2 μm
	CANON EOS 1D Mark III	I^\uparrow ($\text{W m}^{-2} \text{ nm}^{-1} \text{ sr}^{-1}$)	180° fish-eye lens
	RIEGL VQ580	Surface topography	Airborne laser scanner
	AIMMS20	\vec{v}, p	Meteorological measurements
	KT19	T_{surf}	Radiation thermometer

F^\downarrow : downward irradiance, F^\uparrow : upward irradiance, λ : wavelength (indicates spectral quantity), I^\uparrow : reflected radiance, AOD: aerosol optical depth, p : pressure, T : temperature, RH: relative humidity, \vec{v} : wind vector, SSA: specific surface area, ρ_{snow} : snow density, T_{surf} : surface temperature